Inorganic Chemistry

Article

pubs.acs.org/IC

Tuning the Luminescent Properties of Pt(II) Acetylide Complexes through Varying the Electronic Properties of N-Heterocyclic Carbene Ligands

Yuzhen Zhang, Jessica Clavadetscher, Michael Bachmann, Olivier Blacque, and Koushik Venkatesan*

Institute of Inorganic Chemistry, University of Zürich, Winterthurerstrasse 190, CH-8057 Zürich, Switzerland

Supporting Information

ABSTRACT: This Article reports the synthesis, structural characterization, electrochemistry, and photophysical investigations of five groups of luminescent Pt(II) alkynyl complexes bearing N-heterocyclic carbene (NHC) ligands with varying electronic properties. Complexes of the type [Pt(**pmdb**)(C≡CR)$_2$] **1a−c**, [Pt(**pm2tz**)(C≡CR)$_2$] **2a−d**, [Pt(**pm3tz**)(C≡CR)$_2$] **3a−c**, [Pt(**ppim**)(C≡CR)$_2$] **4**(**a**, **b**, **e**), and [Pt(**ppbim**)(C≡CR)$_2$] **5**(**a**, **b**, **e**), where pmdb =1,1′-dipentyl-3,3′-methylene-dibenzimidazoline-2,2′-diylidene, pm2tz = 1,1′-dipentyl-3,3′-methylene-di-1,2,4-triazoline-5,5′-diylidene, pm3tz = 1,1′-dipentyl-3,3′-methylene-di-1,3,4-triazoline-5,5′-diylidene, ppim = 3-pentyl-1-picolylimidazoline-2-ylidene, and ppbim = 3-pentyl-1-picolylbenzimidazoline-2-ylidene, and R = 4-C_6H_4F, C_6H_5, 4-C_6H_4OMe, $SiMe_3$, and 4-$C_6H_4N(C_6H_5)_2$, were prepared, and the consequences of the electronic properties of the NHC ligands on the phosphorescent emission efficiencies were studied. Moreover, the emission quantum efficiencies of the previously reported complexes [Pt(**pmim**)(C≡CR)$_2$] where **pmim** = 1,1′-dipentyl-3,3′-methylene-diimidazoline-2,2′-diylidene and R = 4-C_6H_4F **6a**, C_6H_5 **6b**, and 4-C_6H_4OMe **6c** were also recorded in neat solid and in 10 wt % PMMA film. The square planar coordination geometry with the alkynyl ligands in *cis* configuration was corroborated for selected complexes by single crystal X-ray diffraction studies. The observed moderate difference in emission efficiencies of the bis-carbene complexes **6a−c**, **1a−c**, **2a−c**, and **3a−c** in conjunction with the decreasing electron-donating nature of the NHC ligands, **pmim** > **pmdb** > **pm2tz** ≈ **pm3tz**, can be attributed to the slight modification of the triplet emission parentage among the different complexes. The quantum efficiencies of complexes **4**(**a**, **b**) and **5**(**a**, **b**) bearing pyridyl-NHC ligand were significantly low in comparison to the bis-carbene complexes owing to the significant change in the charge transfer character of the triplet manifold. Complexes **4e** and **5e** bearing diarylamine phenylacetylenes display high ϕ_{em} of 27% and 33% in 10 wt % PMMA film, respectively.

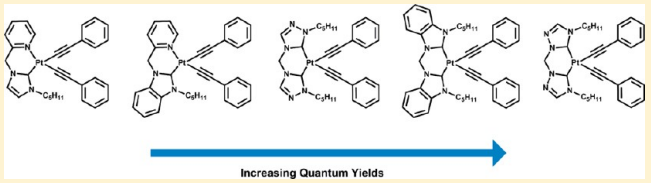

INTRODUCTION

Platinum(II) triplet emitters have been intensively investigated due to their interesting photophysical properties and their application in OLEDs.[1] In particular, high phosphorescent quantum efficiency combined with microsecond excited state lifetime has been successfully achieved by utilizing cyclometalating ligands as part of the molecular scaffold.[1f,2] Although highly efficient green and red emitters have been achieved and widely explored, stable and highly efficient deep blue emitters based on Pt(II) complexes remain scarce and less explored.[3] Recently, the groups of Strassner,[4] Li,[2c,5] and Wang[6] have reported on the development of blue emitters utilizing cyclometalated NHC ligand as part of the coordination sphere of the Pt(II) complexes. The main reason for the high quantum efficiency displayed by the cyclometalated NHC complexes can be ascribed to the strong ligand field (LF) strength that effectively separates the closely associated emitting states and the nonradiative d−d excited states by raising the energy of the nonradiative metal-centered d−d excited states.[1j,7] Around the same time, our group also independently reported the first series of room temperature phosphorescent NHC Pt(II) acetylide [Pt(**pmim**)(C≡CR)$_2$] (**pmim** = 1,1′-dipentyl-3,3′-methylene-diimidazoline-2,2′-diylidene).[8] Some of the complexes displayed deep blue emission in solution albeit with low quantum efficiencies. The quantum efficiencies of the complexes could not be improved by altering the electronic nature of the alkynyl ligands, since the emission energies were significantly affected upon changing the substituents on the alkynyl ligands. On the basis of these results, it was surmised that employing a strategy that involved the altering of the donor properties of the NHC ligand would allow tuning of emission quantum yields of these classes of molecules in the deep blue region without significantly shifting the emission energies. The systematic variation of the NHC donor properties was expected to affect the extent to which the low-lying d−d states are raised in energy with respect to the emissive states and as a consequence impact the luminescent properties.

In this context, we report the preparation and photophysical investigations of five new groups of complexes [Pt(**pmdb**)(C≡CR)$_2$] **1a−c**, [Pt(**pm2tz**)(C≡CR)$_2$] **2a−d**, [Pt(**pm3tz**)(C≡CR)$_2$] **3a−c**, [Pt(**ppim**)(C≡CR)$_2$] **4**(**a**, **b**, **e**), and [Pt(**ppbim**)(C≡CR)$_2$] **5**(**a**, **b**, **e**). The emission properties of

Received: July 17, 2013
Published: January 6, 2014

   dx.doi.org/10.1021/ic401841n | *Inorg. Chem.* 2014, 53, 756−771

Scheme 1. Synthetic Procedure for Pt(II) Acetylide Complexes Bearing Different NHC Ligands

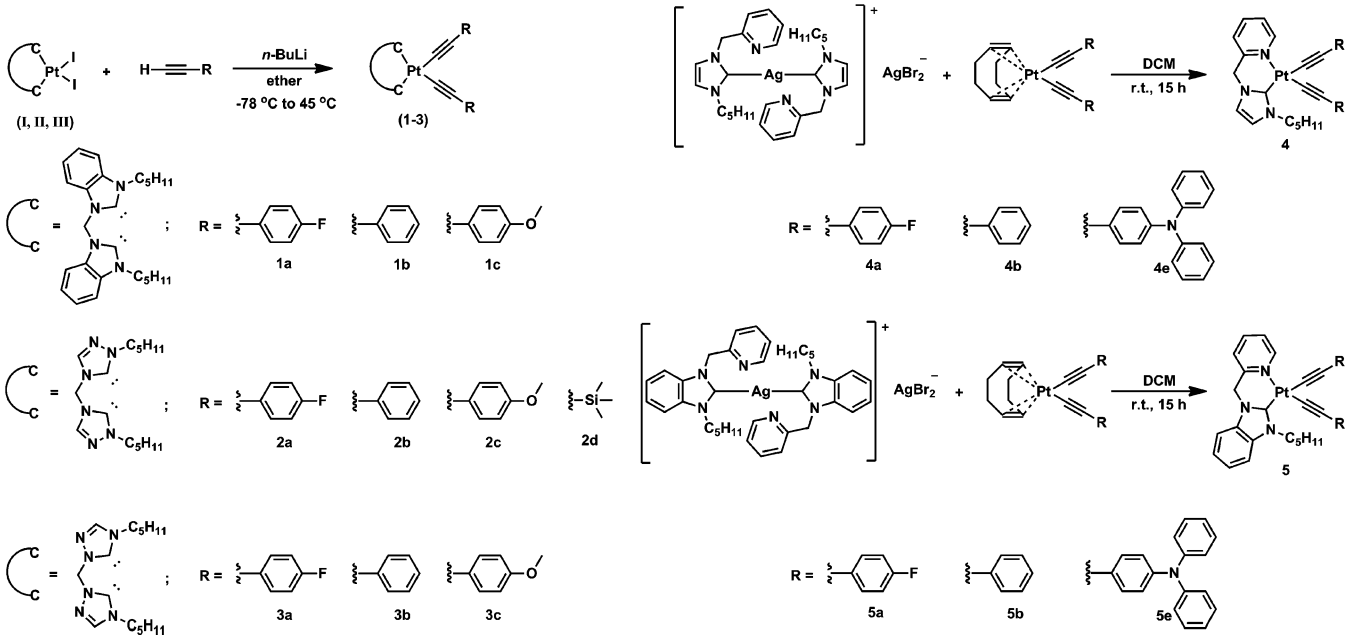

the previously reported complexes [Pt(**pmim**)(C≡CR)$_2$] **6a**–**c** in neat solid and in 10 wt % PMMA film were examined. All five groups of complexes **1**–**5** were synthesized to assess the effect of the electronic nature of the NHC ligands on the emission quantum yields. Complexes **4e** and **5e** bearing the diarylaminephenylacetylene ligand exhibited green emission with high quantum efficiencies of 27% and 33% in 10 wt % PMMA film. On the basis of the different emission quantum yields of the above series of complexes bearing electronically different bidentate NHC ligands, the results are suggestive of the significant role of the electronic nature of the NHC ligands on the excited state responsible for the emission.

RESULTS AND DISCUSSION

Synthesis and Characterization. The precursor complexes **I**, **II**, and **III** were prepared by slight modification of previous literature reports.[4a,8,9] The corresponding targeted dialkynyl complexes **1a**–**c**, **2a**–**d**, and **3a**–**c** were synthesized in yields of 18–87% by reacting the precursor complexes **I**, **II**, and **III** with lithiated acetylenes in dry Et$_2$O at 45 °C in a sealed Schlenk flask (Scheme 1, left). A different strategy was followed for the synthesis of complexes **4**(**a**, **b**, **e**) and **5**(**a**, **b**, **e**). Treatment of the silver salts of **ppim** and **ppbim** with [Pt(COD)(C≡CR)$_2$] in dichloromethane at room temperature (Scheme 1, right) gave the corresponding dialkynyl complexes directly in good yields after purification by chromatography on silica gel.[10] Due to partial decomposition of **4e** and **5e** during column chromatography, there was slight loss of the compounds during purification.

All the prepared complexes were characterized by ^{1}H NMR, ^{13}C NMR, elemental analyses, and FT-IR spectroscopy. Single crystal X-ray diffraction studies were carried out for complexes **I**, **1a**, **1b**, and **2a**. Although no single crystals suitable for the diffraction studies could be obtained in the case of complexes **3a**–**3c**, the distinct chemical shifts in the ^{13}C NMR spectra for the NCH$_2$N bridging the two triazole units in these complexes provide a strong indication of the structure being different from complexes **2a**–**2c**. The characteristic resonances observed in the ^{13}C NMR spectra at around 170 ppm for the coordinated carbene ligand and at 102 and 109 ppm for the alkynyl ligand along with the stretching vibration bands at 2100 cm^{-1} in the IR spectra further confirmed the coordination of the acetylide ligand.

Crystal Structure Determination. Single crystals of **I**, **1a**, **1b**, and **2a** were obtained by slow evaporation of a mixture of CH$_2$Cl$_2$/pentane, and the plots of the molecular structures are shown in Figure 1. The crystallographic details are summarized in Supporting Information Table S1, and selected bond lengths and angles are listed in Table 1. All the four Pt(II) complexes exhibit distorted square planar coordination geometry with two alkynyl ligands disposed *cis* to each other. The dihedral angles of 52.9(2)° for **I**, 40.3(2)–42.5(1)° for **1a**, 40.96(4)–46.20(1)° for **1b**, and 38.9(3)–42.3(2)° for **2a**, dissecting the NHC plane and the distorted Pt square plane, were found to be strikingly different from each other. The bond length of 1.976(5) Å for the Pt–C$_{carb}$ bond in the precursor complex **I** was found to be shorter than those in **1a** (2.027(6) and 2.033(6) Å) and **1b** (2.0307(6), 2.0327(7), 2.0052(6), and 2.0223(6) Å). The C$_{alk}$–Pt–C$_{alk}$ angles were found to be strongly varying between the complexes **1a**, **1b**, and **2a** which are 86.7(3)° for **1a**, 85.6(3) and 86.68(3)° for **1b**, and 90.4(3)° and 91.8(3)° for **2a**. The smaller C$_{alk}$–Pt–C$_{alk}$ angle found for **1a** in comparison to **2a** could be attributed to the large extrusion force of **pmdb**.

Photophysical Properties. The UV–vis absorption spectra of complexes **1a**–**c**, **2a**–**d**, and **3a**–**c** show absorption bands in the ranges 250–295 and 300–340 nm with molar extinction coefficients in the range of 10^4 M^{-1} cm^{-1} in dichloromethane except in the case of complex **2d**, which was found to possess low extinction coefficient (Figures 2–4, Supporting Information Figure S1). The absorption maxima of the complexes **1a**, **1b**, and **1c** bearing the **pmdb** ligand and electronically different alkynyls display modest bathochromic shifts going from **1a** to **1b**, but a significant shift to lower energy was observed in the case of **1c**. The extent of the observed red shift is consistent with the increasing electron donating nature of the alkynyl in the order F < H < OMe. A

dx.doi.org/10.1021/ic401841n | Inorg. Chem. 2014, 53, 756–771

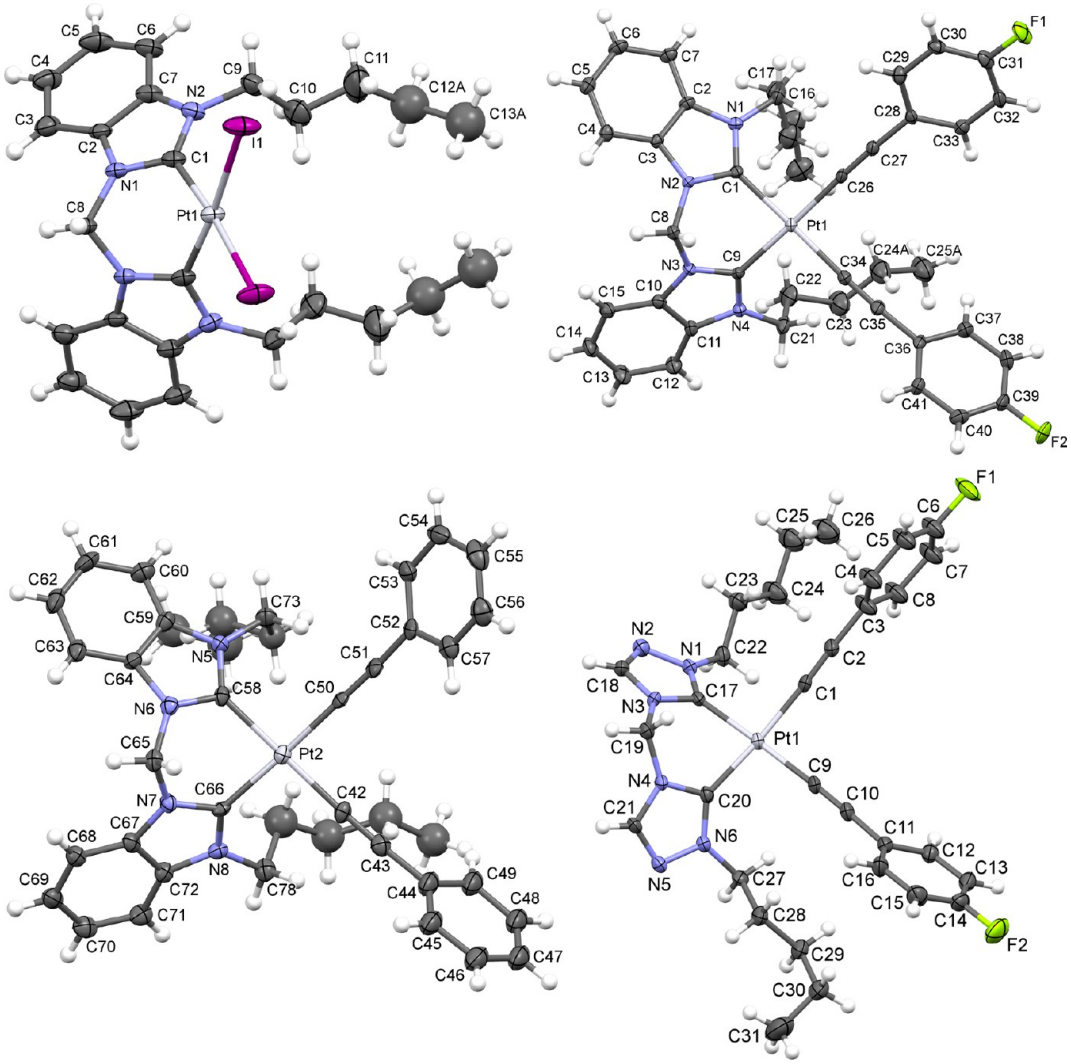

Figure 1. Molecular structures of **I** (top left), **1a** (top right), **1b** (bottom left), and **2a** (bottom right) with a selective atomic numbering scheme. Thermal ellipsoids are drawn at the 30% probability level. Disorders and solvent molecules are omitted for clarity, and the hydrogen atoms are presented as white spheres.

strong hypsochromic shift of the absorption band was found for complexes **2b** and **3b** with respect to **1b**. The shifts are consistent with the decreasing electron donating nature of the NHC ligand in the order **pmdb** < **pm2tz** < **pm3tz**.[11] On the basis of the experimental studies and DFT/TDDFT calculations, the natures of the transitions responsible for the low energy absorption bands in these complexes are assigned to a mixture of metal-perturbed intraligand ^{1}ILCT($\pi_{alk} \rightarrow \pi^*_{alk}$), metal-perturbed ligand-to-ligand ^{1}LLCT($\pi_{alk} \rightarrow \pi^*_{carb}$), and metal-to-ligand ^{1}MLCT(Pt→π^*_{alk}) transitions. In the higher energy part of the absorption spectrum, only one prominent band was observed for complexes **2a**−**c** and **3a**−**c** with extinction coefficients of 5 × 10^4 M^{-1} cm^{-1}, and the parentage of this band is ascribed to a metal-perturbed intraligand ^{1}ILCT ($\pi_{alk} \rightarrow \pi^*_{alk}$) transition. However, in comparison to the complexes **2a**−**c** and **3a**−**c**, complexes **1a**−**c** showed an additional absorption band at a higher energy. The origin of the band is assigned to transitions involving a metal-perturbed ^{1}ILCT ($\pi_{alk} \rightarrow \pi^*_{carb}$). Complexes **4b** and **5b** possess a low energy absorption band that is bathochromically shifted by 9 nm (824 cm^{-1}) in comparison of complexes **2b** and **3b** but only 2 nm (177 cm^{-1}) hypsochromic shift than **1b** owing to the influence of NHC-pyridyl ligand (Figures 3 and 4). An additional band appears as a shoulder between the high and low energy absorption bands which is tentatively assigned to intraligand ^{1}IL ($\pi_{pyr} \rightarrow \pi^*_{pyr}$) transition. The absorption spectrum of complexes **4e** and **5e** exhibits one main strong absorption band at 330 nm with extinction coefficients around 6 × 10^4 M^{-1} cm^{-1} (Figures 3 and 4), and the nature of the transition is assigned as a mixture of ^{1}IL, ^{1}LLCT, and ^{1}MLCT.

In order to obtain more information on the nature of the charge-transfer state, solvatochromic behavior of the representative molecules **1b**, **2b**, **3b**, **4b**, and **5b** in toluene, CH_2Cl_2, THF, CH_3CN, and MeOH (Figure 5, Supporting Information Figures S2−S5) was studied. The solvent dependent changes of the lowest-energy absorption maxima were observed for all of the five complexes. They show negative solvatochromic behavior with shifts ranging between 11 and 27 nm (~1039−2252 cm^{-1}). Significant shifts were observed particularly for complexes **4b** and **5b** bearing the pyridyl-NHC ligand. The negative solvatochromic behavior indicates a more polar ground state than the excited state.[1k,12] This is further substantiated by the estimation of the dipole moment by TD-DFT calculations for complexes **1b**−**5b**. Similar behavior

dx.doi.org/10.1021/ic401841n | *Inorg. Chem.* 2014, 53, 756−771

Table 1. Selected Bond Lengths and Angles for Complexes I, 1a, 1b, and 2a

	bond length (Å)		bond angle (deg)
Complex **I**			
C1−Pt1	1.976(5)	C1−Pt1−C1^{i}	83.6(3)^{a}
I1−Pt1	2.6534(4)	I1−Pt1−I1^{i}	89.57(2)
Complex **1a**			
C1−Pt1	2.027(6)	C1−Pt1−C9	85.0(2)
C9−Pt1	2.033(6)	C1−Pt1−C26	93.5(2)
C26−Pt1	2.013(7)	C9−Pt1−C34	94.8(2)
C34−Pt1	2.008(7)	C26−Pt1−C34	86.7(3)
Complex **1b** (Two Crystallographically Independent Molecules)			
C1−Pt1	2.011(10)	C1−Pt1−C9	85.6(3)
C9−Pt1	2.0220(6)	C1−Pt1−C17	94.5(3)
C17−Pt1	2.0307(6)	C9−Pt1−C25	94.25(3)
C25−Pt1	2.0327(7)	C17−Pt1−C25	85.63(3)
C42−Pt2	1.9862(6)	C42−Pt2−C50	86.68(3)
C50−Pt2	2.0114(7)	C42−Pt2−C66	94.90(3)
C58−Pt2	2.0052(6)	C50−Pt2−C58	93.12(3)
C66−Pt2	2.0223(6)	C58−Pt2−C66	85.29(2)
Complex **2a** (Two Crystallographically Independent Molecules)			
C1−Pt1	2.006(8)	C1−Pt1−C9	90.4(3)
C9−Pt1	2.000(8)	C1−Pt1−C17	91.7(3)
C17−Pt1	2.022(7)	C9−Pt1−C20	92.1(3)
C20−Pt1	2.018(8)	C17−Pt1−C20	85.6(3)
C32−Pt2	2.026(10)	C32−Pt2−C40	91.8(3)
C40−Pt2	2.008(9)	C32−Pt2−C48	91.1(3)
C48−Pt2	2.014(8)	C40−Pt2−C51	91.8(3)
C51−Pt2	2.020(9)	C48−Pt2−C51	85.1(3)

^{a}Symmetry code: i = $x, y, -z + {}^{3}/_{2}$.

has been previously reported in the case of metal dithiolate complexes.[12a] Since the evaluated complexes bearing the same alkynyl but different NHC ligand show a different extent of shifts, the nature of the charge transfer excitation could be composed of varying degrees of metal perturbed ^{1}LLCT and ^{1}MLCT.

The phosphorescence emission was measured in deaerated dichloromethane at room temperature (r.t.), and only complexes **1a−c**, **2a**, **2c** and **3a−c** exhibited emission (Supporting Information Figures S6−S8) in solution that can be quenched by oxygen. The emission profiles of the complexes **1a−c** and **3a−c** were broad and structureless, and their emission maxima were in the range 430−450 nm. The emission energy displayed changes reflecting the different electronic properties of the alkynyl ligand (F < H < OMe). Complexes **2b**, **2d**, **4a**, **4b**, **4e**, **5a**, **5b**, and **5e** did not display any observable emission in fluid solution at r.t., and the possible reason for this behavior is ascribed to solvent effects and self-quenching. At 77 K, in the frozen glass state, all complexes exhibit intense and well-structured phosphorescence emission in 2-MeTHF except in the case of complex **2d** for which no noticeable emission was observed (Supporting Information Figures S9−S13). We conclude that the presence of trimethylsilyl group in **2d** leads to an increase in the energy gap of ($\pi_{alk} \rightarrow \pi^{*}_{alk}$) further resulting in a nonradiative decay of the excited state. The phosphorescence emission maxima for the complexes at 77 K were in the range 430−440 nm with structured bands that are typically characteristic of ^{3}ILCT($\pi_{alk} \rightarrow \pi^{*}_{alk}$). Complexes **4e** and **5e** display emission at a lower energy around 480 nm consistent with the strong electron donating nature of the diarylaminephenylacetylene. The solid state emission properties

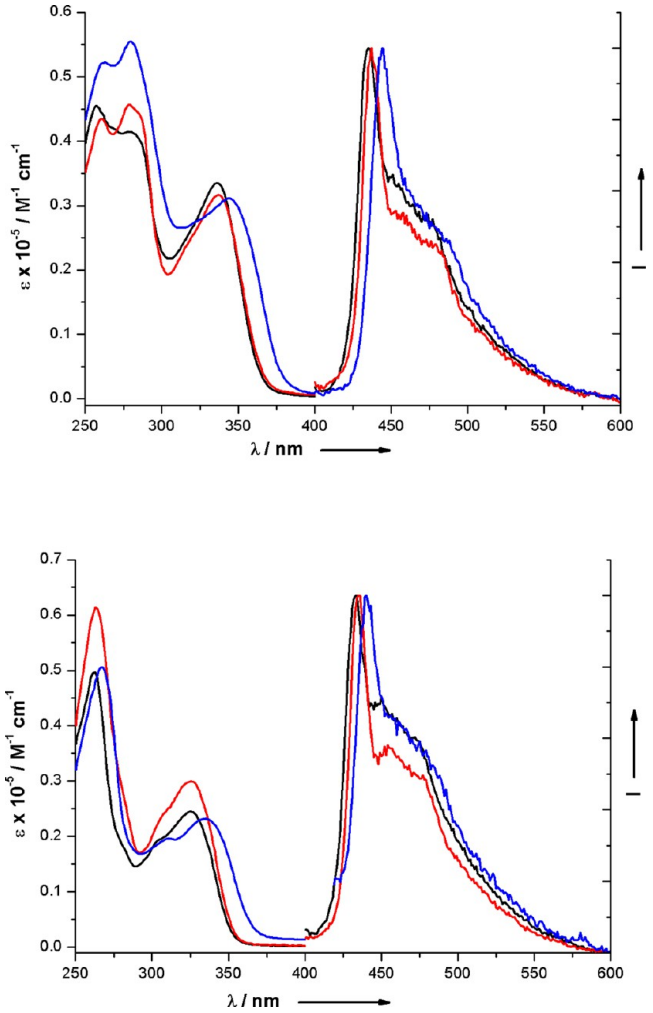

Figure 2. (Left) Electronic absorption spectra of **1a** (black), **1b** (red), **1c** (blue) in DCM, and normalized emission spectra of **1a** (black), **1b** (red), **1c** (blue) in 10 wt % PMMA film. (Right) Electronic absorption spectra of **2a** (black), **2b** (red), **2c** (blue) in DCM, and normalized emission spectra of **2a** (black), **2b** (red), **2c** (blue) in 10 wt % PMMA film.

of the complexes were investigated in neat solid and in 10 wt % PMMA film. The emission spectra of all the complexes except **2d** are shown in Figures 2−4. In contrast to the moderate to good luminescence observed for the complexes in 10 wt % PMMA, the luminescence was found to be very weak in neat solid. The emission wavelength maxima of the complexes appear quite close in the different measured medium (solution, neat solid, 10% PMMA, and 77 K frozen matrix), albeit with a small blue shift in the 77 K frozen matrix due to the enhanced rigidochromic effect. The strongly correlated emission maxima among the different media along with the absence of concentration dependent emission wavelength changes are strongly suggestive of low quantum yields in neat solid versus the emission of the complexes doped in PMMA being due to a self-quenching process rather than an excimer formation.[13] Also, any Pt···Pt interactions can be ruled out, since the Pt···Pt distances for the complexes **1a**, **1b**, and **2a** were found to be 7.7164 (6), 5.7262(6), and 7.8761(5) Å, respectively.

Due to the weak luminescence in fluid solution, emission quantum yields were not measured in solution, and instead, measurements were made both in the neat solid and 10 wt %

dx.doi.org/10.1021/ic401841n | Inorg. Chem. 2014, 53, 756−771

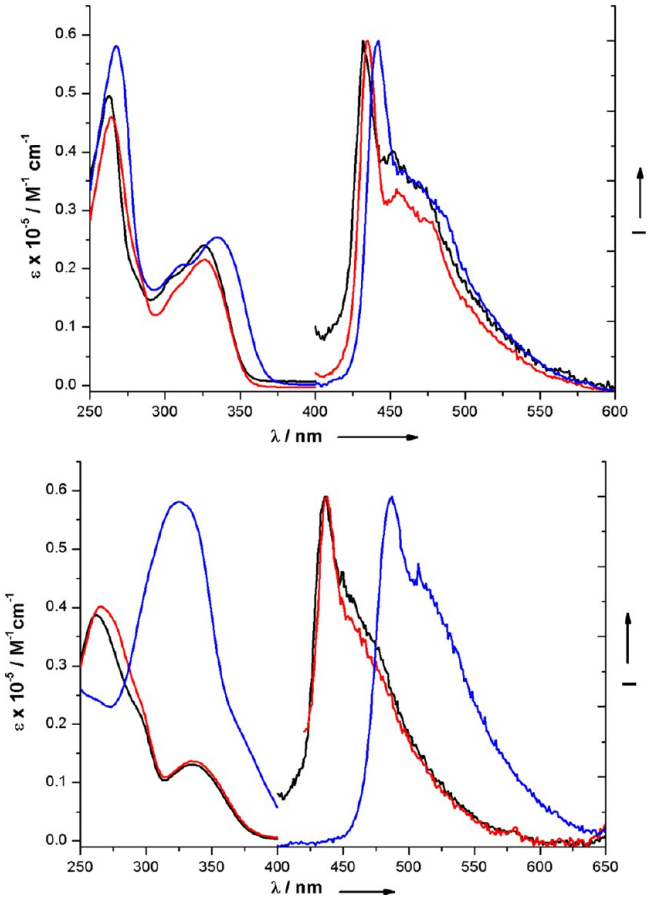

Figure 3. (Left) Electronic absorption spectra of **3a** (black), **3b** (red), **3c** (blue) in DCM, and normalized emission spectra of **3a** (black), **3b** (red), **3c** (blue) in 10 wt % PMMA film. (Right) Electronic absorption spectra of **4a** (black), **4b** (red), **4e** (blue) in DCM, and normalized emission spectra of **4a** (black), **4b** (red), **4e** (blue) in 10 wt % PMMA film.

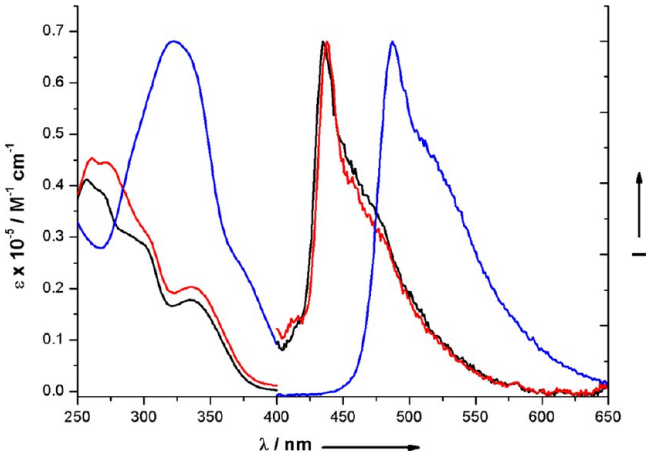

Figure 4. Electronic absorption spectra of **5a** (black), **5b** (red), **5e** (blue) in DCM, and normalized emission spectra of **5a** (black), **5b** (red), **5e** (blue) in 10 wt % PMMA film.

PMMA film. Solid-state quantum yields were also recorded for the previously reported complexes [Pt(pmim)C≡CR] (R = 4-C_6H_4F **6a**, C_6H_5 **6b**, 4-C_6H_4OMe **6c**) by our group for comparison reasons (Table 2). Owing to the strong aggregation of the complexes in the neat solid, the quantum yields were

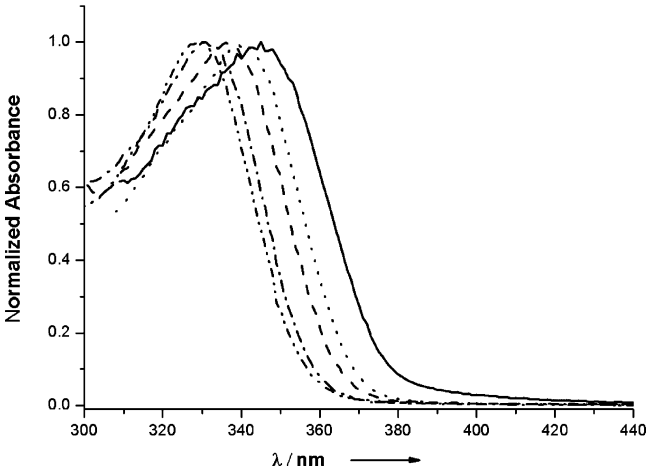

Figure 5. UV−vis absorption spectra of **1b** in toluene (—), THF (···), CH_2Cl_2 (---), CH_3CN (−·−), and MeOH(−···−).

below 1%, but they were found to be as high as 33% in 10 wt % PMMA film. For complexes **1a−c**, **2a−c**, **3a−c**, and **6a−c** the quantum yields were in the range 14−33%. It was observed that the complexes **1b**, **2b**, **3b**, and **6b** bearing phenylacetylene ligand always displayed lower quantum yields than the rest of the complexes bearing 4-florophenylacetylene (**1a**, **2a**, **3a**, and **6a**) and 4-methoxylphenylacetylene (**1c**, **2c**, **3c**, and **6c**) as ancillary ligands. While the complexes **4a**, **4b**, **5a**, and **5b** exhibited a low quantum yield of 5−8%, complexes **4e** and **5e** displayed higher quantum efficiencies of 27% and 33% albeit at lower emission energies due to the electronically different alkynyl ligand. The comparatively low quantum yields of complexes **4a**, **4b**, **5a**, and **5b** are tentatively ascribed to the competing nonradiative decay of low-lying d−d states caused by the less strongly electron-donating pyridyl-NHC ligand. Further experimental studies are required to ascertain the nature of the processes contributing to the nonradiative process in these complexes, which is currently in progress.

Electrochemical Properties. The cyclic voltammetric data for the complexes are listed in Table 3. All the complexes were measured in DCM using 0.1 M [*n*-Bu_4N][PF_6] as supporting electrolyte, and ferrocenium/ferrocene (Fc^+/Fc) was used as an internal reference for calibration. Although no reduction wave was observed for any of the complexes including complexes **4**(**a**, **b**, **e**) and **5**(**a**, **b**, **e**) bearing pyridyl group in the ligand scaffold on scanning up to −2.18 V in DCM, an irreversible reduction wave was observed in DMF in the range −2.53 to −2.44 V (see Supporting Information Table S2). This pyridyl ligand based reduction was found to be shifted to more negative potentials in comparison to the polypyridyl Pt(II) acetylide complexes.[12b,14] This observation is similar to the behavior of the previously reported complexes [Pt(**pmim**)(C≡CR)$_2$] and [Pt(phospine)$_2$(C≡CR)$_2$].[15] However, it is quite different from the reported polypyridyl Pt(II) acetylide complexes which have one or more reversible reduction waves attributed to the polypyridyl ligand. Complexes **1a−c**, **2a−d**, and **3a−c** displayed only one oxidation wave, and the oxidation potential varied depending on both the nature of the alkynyl ligand and the NHC ligand. For example, in complexes **1a−c**, the oxidation potential decreased with increasing electron richness of the acetylide. This trend is consistent with the energy of the emission. In comparison of the oxidation potential among the complexes **1a** (+0.77 V), **2a** (+0.80 V),

dx.doi.org/10.1021/ic401841n | *Inorg. Chem.* 2014, 53, 756−771

Table 2. Photophysical Properties of Complexes 1a–c, 2a–d, 3a–c, 4(a, b, e), 5(a, b, e), and 6a–c

complex	absorption (CH_2Cl_2)	medium (T/K)	emission λ_{max}/nm (τ_0/ μs)	ϕ_{em} (%)	k_r [$\times 10^3$ s^{-1}]	k_{nr} [$\times 10^5$ s^{-1}]
1a	257 (45 521), 280 (41 444), 337 (33 479)	CH_2Cl_2 (298)	436, 523 sh			
		glass (77)	433, 450 sh, 475 sh			
		solid (298)	435, 451, 467	1.0		
		PMMA (298)	437, 473 (3.50)	19.3	55.1	2.3
1b	261 (43 480), 280 (45 723), 337 (31 660)	CH_2Cl_2 (298)	437, 530 sh			
		glass (77)	437, 459 sh, 484 sh			
		solid (298)		<1		
		PMMA (298)	437, 480 (1.94)	14.6	75.2	4.4
1c	263 (55 241), 280 (55 483), 344 (31 109)	CH_2Cl_2 (298)	445, 541 sh			
		glass (77)	437, 455 sh, 476 sh			
		solid (298)		<1		
		PMMA (298)	445, 483 sh (2.20)	22.8	103.6	3.5
2a	263 (44 668), 326 (24 497)	CH_2Cl_2 (298)	437, 533			
		glass (77)	427, 447 sh, 470			
		solid (298)		<1		
		PMMA (298)	436, 478 (1.23)	17.6	143.1	6.7
2b	263 (61 370), 326 (29 949)	CH_2Cl_2 (298)				
		glass (77)	432, 454 sh, 478 sh			
		solid (298)		<1		
		PMMA (298)	436, 478 sh (1.47)	14.1	95.9	5.8
2c	267 (50 594), 335 (23 223)	CH_2Cl_2 (298)	445, 545 sh			
		glass (77)	435, 461 sh, 483 sh			
		solid (298)		<1		
		PMMA (298)	440, 477 sh (0.10)	32.8	3280	67.2
2d	272 (20 951), 315 (16 973)	CH_2Cl_2 (298)				
		glass (77)				
		solid (298)				
		PMMA (298)				
3a	263 (49 662), 326 (23 962)	CH_2Cl_2 (298)	435, 512 sh			
		glass (77)	426, 447, 465			
		solid (298)		<1		
		PMMA (298)	432, 453 sh (0.03)	19.3	6433	268.9
3b	264 (46 001), 326 (21 497)	CH_2Cl_2 (298)	435, 521 sh			
		glass (77)	432, 453 sh, 475 sh			
		solid (298)		<1		
		PMMA (298)	435, 457 sh (1.85)	17.7	95.7	4.4
3c	267 (58 124), 335 (25 367)	CH_2Cl_2 (298)	442, 515 sh			
		glass (77)	436, 456 sh, 481 sh			
		solid (298)		<1		
		PMMA (298)	442, 473 sh (2.9)	28.1	96.9	2.5
4a	262 (38 656), 292 (23 122), 335 (13 123)	CH_2Cl_2 (298)				
		glass (77)	426, 448 sh, 476 sh			
		solid (298)		<1		
		PMMA (298)	437, 475 sh (1.56)	5.6	35.9	6.0
4b	265 (40 143), 297 (22 919), 335 (13 640)	CH_2Cl_2 (298)				
		glass (77)	430, 452, 478			
		solid (298)		<1		
		PMMA (298)	438, 472 (1.98)	5.0	25.2	4.8
4e	325 (58 013), 375 (17 303)	CH_2Cl_2 (298)				
		glass (77)	478, 490 sh, 521 sh			
		solid (298)		<1		
		PMMA (298)	487, 507 sh (2.16)	26.6	123.1	3.4
5a	257 (41 178), 300 (28 590), 335 (17 794)	CH_2Cl_2 (298)				
		glass (77)	427, 446, 484 sh			
		solid (298)		<1		
		PMMA (298)	436, 478 sh (1.82)	7.7	42.3	5.1
5b	261 (46 426), 301 (31 047), 335 (20 351)	CH_2Cl_2 (298)				
		glass (77)	431, 450 sh, 486 sh			
		solid (298)		<1		
		PMMA (298)	438, 483 sh (1.94)	8.1	41.7	4.7
5e	322 (68 108), 381 (20 633)	CH_2Cl_2 (298)				

dx.doi.org/10.1021/ic401841n | *Inorg. Chem.* 2014, 53, 756–771

Table 2. continued

complex	absorption (CH_2Cl_2)	medium (T/K)	emission λ_{max}/nm (τ_0/ μs)	ϕ_{em} (%)	k_r [$\times 10^3$ s^{-1}]	k_{nr} [$\times 10^5$ s^{-1}]
		glass (77)	479, 508 sh, 530 sh			
		solid (298)	485, 517 sh	1.1		
		PMMA (298)	488, 520 sh (2.59)	32.7	126.2	2.6
6a[a]	264 (48 600), 324 (29 400)	CH_2Cl_2 (298)	440, 475 sh			
		glass (77)	429, 455 sh			
		solid (298)	437, 471 sh	2.9		
		PMMA (298)	439, 473 sh (3.02)	18	59.2	2.7
6b[a]	266 (51 700), 330 (28 600)	CH_2Cl_2 (298)	442, 482 sh			
		glass (77)	437, 456 sh,			
		solid (298)	439, 478 sh	4.8		
		PMMA (298)	441, 480 sh	17.7		
6c[a]	323 (44 600)	CH_2Cl_2 (298)	447, 475 sh			
		glass (77)	440, 484 sh			
		solid (298)	443, 469 sh	2.0		
		PMMA (298)	445, 473 sh	17.7		

[a]Data from ref 8.

Table 3. Electrochemical Data[a] for Complexes 1a−c, 2a−d, 3a−c, 4(a, b, e), and 5(a, b, e)

complex	E_{ox} (V)
1a	+0.77
1b	+0.76
1c	+0.50
2a	+0.80
2b	+0.75
2c	+0.53
2d	+1.19
3a	+0.82
3b	+0.82
3c	+0.57
4a	+0.73
4b	+0.72
4e	+0.34, +0.56 (quasireversible)
5a	+0.77
5b	+0.77
5e	+0.24, +0.58 (quasireversible)

[a]Scan rate = 100 mV s^{-1} in 0.1 M [n-Bu_4N][PF_6] (Au electrode; E vs Fc^+/ Fc; 20 °C; DCM).

and **3a** (+0.82 V), the potential was found to increase with the decreasing electron-donating character of the NHC ligand in the order **pmdb** < **pm2tz** < **pm3tz**. A significant increase in the oxidation potential of +1.19 V was observed for complex **2d**, strongly indicating a low-lying HOMO and as a result showing no emission in all kind of medium at room temperature. Complexes **4a**, **4b**, **5a**, and **5b** also exhibit one oxidative wave at similar potentials in comparison to the other three groups of complexes. Complexes **4e** and **5e** exhibit one irreversible oxidation wave at +0.34 and +0.24 V and additionally one quasireversible wave at +0.56 and +0.58 V, respectively. However in DMF, two quasireversible waves at +0.28 V and +0.44 V were observed for complex **4e** and at +0.29 and 0.45 V for complex **5e** (Supporting Information Table S2). The first oxidation wave was ascribed to the oxidation of C≡CR, and the second quasireversible waves are likely to be triphenylamine-based oxidation with some mixing of metal-centered character. The strong shifts in the oxidation potential indicate the relative changes in the positions of the HOMO level among the complexes that affect also the emission energies significantly. The complexes with lower oxidation potentials indicate relatively high lying HOMOs, and these complexes possess better emission quantum yields.

DFT and TD-DFT Calculations. In order to study the luminescent properties of our Pt(II) alkynyl complexes bearing N-heterocyclic carbene ligands, we performed DFT and TD-DFT calculations for **1b−5b** (which bear the same phenylacetylide ligand) with the *Gaussian03* program package.[16] The hybrid functional PBE1PBE[17] (also known as PBE0) in conjunction with the Stuttgart/Dresden effective core potentials (SDD) basis set[18] for the Pt center augmented with one f-polarization function (exponent = 0.993), and the standard 6-31+G(d) basis set[19] for the remaining atoms was applied for all calculations. Full geometry optimizations without symmetry constraints were carried out in the gas phase for the singlet ground states (S_0) and the lowest triplet states (T_1). The optimized geometries S_0 and T_1 were confirmed to be potential energy minima by vibrational frequency calculations at the same level of theory, as no imaginary frequency was found. The first 10 singlet−singlet and singlet−triplet transition energies were computed at the optimized S_0 geometries, by using the time-dependent DFT (TD-DFT) methodology.[20] Solvent effects were taken into account using the conductor-like polarizable continuum model (CPCM)[21] with dichloromethane as solvent for single-point calculations on all optimized gas-phase geometries.

The experimental UV−vis absorption spectra of complexes **1b−5b** in dichloromethane at room temperature show absorption bands in the ranges 260−295 and 325−340 nm. The absorption maxima experimentally observed in the range 325−340 nm for each compound **1b−5b** arise from the overlap of the TD-DFT calculated $S_0 \rightarrow S_1$ and $S_0 \rightarrow S_2$ singlet−singlet transitions (Table 4). The one-electron excitations involved in these transitions are HOMO → LUMO and HOMO − 1 → LUMO. For compounds **1b**, **2b**, and **3b**, the analysis of the frontier molecular orbitals reveals that the low energy absorption band corresponds to a mixture of metal-perturbed ligand-to-ligand $^1LL(\pi_{alk} \rightarrow \pi^*_{carb})$ charge transfer and metal-perturbed intraligand $^1IL(\pi_{alk} \rightarrow \pi^*_{alk})$ charge transfer (Figure 6, Table 5). For compounds **4b** and **5b**, the LUMO is mainly located on the pyridine ligand (72−84%) and shows very small contributions from the carbene ligand (2−8%) and the metal center (7−9%). In the occupied orbitals HOMO and HOMO − 1, the electron density is mainly located on the metal center

dx.doi.org/10.1021/ic401841n | Inorg. Chem. 2014, 53, 756−771

Table 4. Selected Singlet−Singlet (S_0-S_n) and Singlet−Triplet (S_0-T_1) Excited States with TD-DFT/CPCM (in Dichloromethane), Vertical Excitation Energies (nm), Transition Coefficients, Orbitals Involved in the Transitions, and Oscillator Strengths f for Compounds 1b−5b (with $f > 0.07$)

	1b	2b	3b	4b	5b
exp abs λ_{max} [a]	337, 280, 261	326, 263	326, 264	335, 297, 265	335, 301, 261
S_0-S_n	$n = 1$	$n = 1$	$n = 1$	$n = 1$	$n = 1$
	352 ($f = 0.258$)	336 ($f = 0.149$)	336 (0.121)	376 (0.093)	372 (0.158)
	H − 1 → LUMO (0.69)	HOMO → LUMO (0.69)	HOMO → LUMO (0.69)	HOMO → LUMO (0.57)	H − 1 → LUMO (0.54)
				H − 1 → LUMO (0.42)	HOMO → LUMO (0.45)
	$n = 2$	$n = 2$	$n = 2$	$n = 2$	$n = 2$
	347 ($f = 0.285$)	329 ($f = 0.290$)	327 (0.229)	362 (0.172)	365 (0.202)
	HOMO → LUMO (0.69)	H − 1 → LUMO (0.70)	H − 1 → LUMO (0.70)	H − 1 → LUMO (0.56)	HOMO → LUMO (0.52)
	$n = 4$	$n = 4$	$n = 3$	$n = 3$	$n = 3$
	309 ($f = 0.274$)	295 ($f = 0.223$)	300 (0.075)	326 (0.099)	327 (0.082)
	H − 3 → LUMO (0.68)	H − 3 → LUMO (0.68)	H − 2 → LUMO (0.69)	H − 2 → LUMO (0.68)	H − 2 → LUMO (0.67)
	$n = 6$	$n = 6$	$n = 4$	$n = 5$	$n = 5$
	295 ($f = 0.317$)	282 ($f = 0.514$)	292 (0.242)	308 (0.323)	315 (0.560)
	H − 1 → L + 1 (0.68)	HOMO → L + 1 (0.55)	H − 3 → LUMO (0.68)	HOMO → L + 1 (0.57)	H − 1 → L + 1 (0.65)
				H − 1 → L + 1 (0.37)	
	$n = 7$		$n = 6$	$n = 8$	$n = 8$
	290 ($f = 0.256$)		277 ($f = 0.544$)	303 (0.389)	300 (0.085)
	HOMO → L + 1 (0.68)		HOMO → L + 1 (0.53)	HOMO → L + 2 (0.55)	H − 1 → L + 2 (0.58)
				H − 1 → L + 2 (0.39)	HOMO → L + 2 (0.39)
	$n = 8$		$n = 9$		
	287 ($f = 0.129$)		266 ($f = 0.412$)		
	HOMO → L + 2 (0.61)		HOMO → L + 2 (0.63)		
exp emiss λ_{max} [b]	437, 480sh	436, 478sh	435, 457sh	438, 472sh	438, 483sh
T_1-S_0	429	424	422	437	438
	HOMO ← LUMO (0.40)	H − 1 ← LUMO (0.41)	H − 1 ← LUMO (0.36)	HOMO ← L + 2 (0.37)	H − 1 ← LUMO (0.28)
	HOMO ← L + 2 (0.34)	HOMO ← L + 1 (0.38)	HOMO ← L + 1 (0.38)	HOMO ← L + 1 (0.22)	H − 1 ← L + 1 (0.27)
				H − 1 ← L + 2 (0.22)	HOMO ← LUMO (0.26)

[a] In dichloromethane. [b] 10 wt % PMMA film.

(13−18%) and on one alkynyl ligand [the alkynyl ligand *trans* to the pyridine ring in HOMO (82−83%)], and the alkynyl ligand *trans* to the carbene in HOMO − 1 (70%) (Figure 7, Table 6). Consequently, the origin of the absorption maxima in **4b** and **5b** is clearly different from those in **1b**−**3b** due to the presence of the pyridine ligand and can be assigned to transitions involving ligand-to-ligand $^1LL(\pi_{alk(trans\ to\ pyr)} \rightarrow \pi^*_{pyr})$ and $^1LL(\pi_{alk(trans\ to\ carb)} \rightarrow \pi^*_{pyr})$ charge transfers as well as metal-to-ligand $^1ML(Pt \rightarrow \pi^*_{pyr})$ charge transfer. The absorption bands observed at higher energies in the range 260−295 nm are produced from the overlap of two to four significant singlet−singlet transitions with oscillator strength f greater than 0.07 (Table 4) involving many frontier orbitals (Supporting Information Figures S14−S18). In all cases, the bands originate with metal-to-ligand $^1ML[Pt \rightarrow \pi^*_{carb}$ (**1b**−**3b**) or $Pt \rightarrow \pi^*_{pyr}$ (**4b**−**5b**)] and ligand-to-ligand $^1LL[\pi_{alk} \rightarrow \pi^*_{carb}$ (**1b**, **5b**), $\pi_{alk} \rightarrow \pi^*_{alk}$ (**2b**−**4b**), or $\pi_{alk} \rightarrow \pi^*_{pyr}$ (**4b**−**5b**)] charge transfers. For compounds **2b** and **3b**, a sizable amount of intraligand $^1ILCT(\pi_{alk} \rightarrow \pi^*_{alk})$ character can also be deduced from the TD-DFT calculations. The origin of the lowest energy abosprtion bands involving more than one transition is quite unique and has only been observed in the case of plaintum(II) diimine diacetylide complexes.[12d]

The lowest singlet−triplet vertical excitation (T_1-S_0) energies obtained by TD-DFT on the ground state structures of **1b**−**5b** are consistent with the experimental solid state emission properties in 10 wt % PMMA film. The calculated values are slightly underestimated by 8−13 nm for **1b**−**3b**, and are in a very good agreement for **4b**−**5b** (Table 4). The promotion of one electron to unoccupied orbitals leads to high-energy electronic excited states, then spin−orbit interaction between excited states operates to induce S → T intersystem crossing to form the corresponding triplet excited states, and geometry relaxation leads to the lowest energy triplet state (emitting state) for which the optimized structure can be determined by DFT calculations. The geometry of the DFT optimized triplet states of **1b**−**5b** corresponds well to the structural distortions expected upon promotion of one electron to the C≡C antibonding or nonbonding LUMO, LUMO + 1, and/or LUMO + 2 from the C≡C bonding HOMO and/or HOMO − 1 (Supporting Information Figures S14−18) as revealed by the contributions of the TD-DFT S_0-T_1 transitions (Table 4). Due to the symmetry of the involved molecular orbitals, the elongation of the C≡C bond associated to the shortening of the Pt−C and $C-C_{Ph}$ bonds occurs only for one alkynyl ligand. Indeed, the Pt−C bond lengths vary from 1.983−1.986 Å in the ground states to 1.926−1.939 Å in the triplet states (maximum deviation of 0.060 Å for **4b**), the C≡C bond lengths increase from 1.226−1.228 Å to 1.266−1.273 Å (maximum deviation of 0.046 Å for **2b** and **3b**), while the $C-C_{Ph}$ bond lengths decrease from 1.424−1.425 Å to 1.356−1.370 Å (maximum deviation of 0.069 Å for **3b**). The second alkynyl ligand remains almost unchanged, the average variation of the corresponding Pt−C, C≡C, and $C-C_{Ph}$ bond distances is 0.003 Å with a maximum deviation of 0.012 Å for the Pt−C bond length in **4b** (alkynyl *trans* to pyridine ligand). For the unsymmetric molecules **4b** and **5b**, it is important to note that the ^{3}ILCT is likely to take place from the alkynyl *cis* to the

dx.doi.org/10.1021/ic401841n | Inorg. Chem. 2014, 53, 756−771

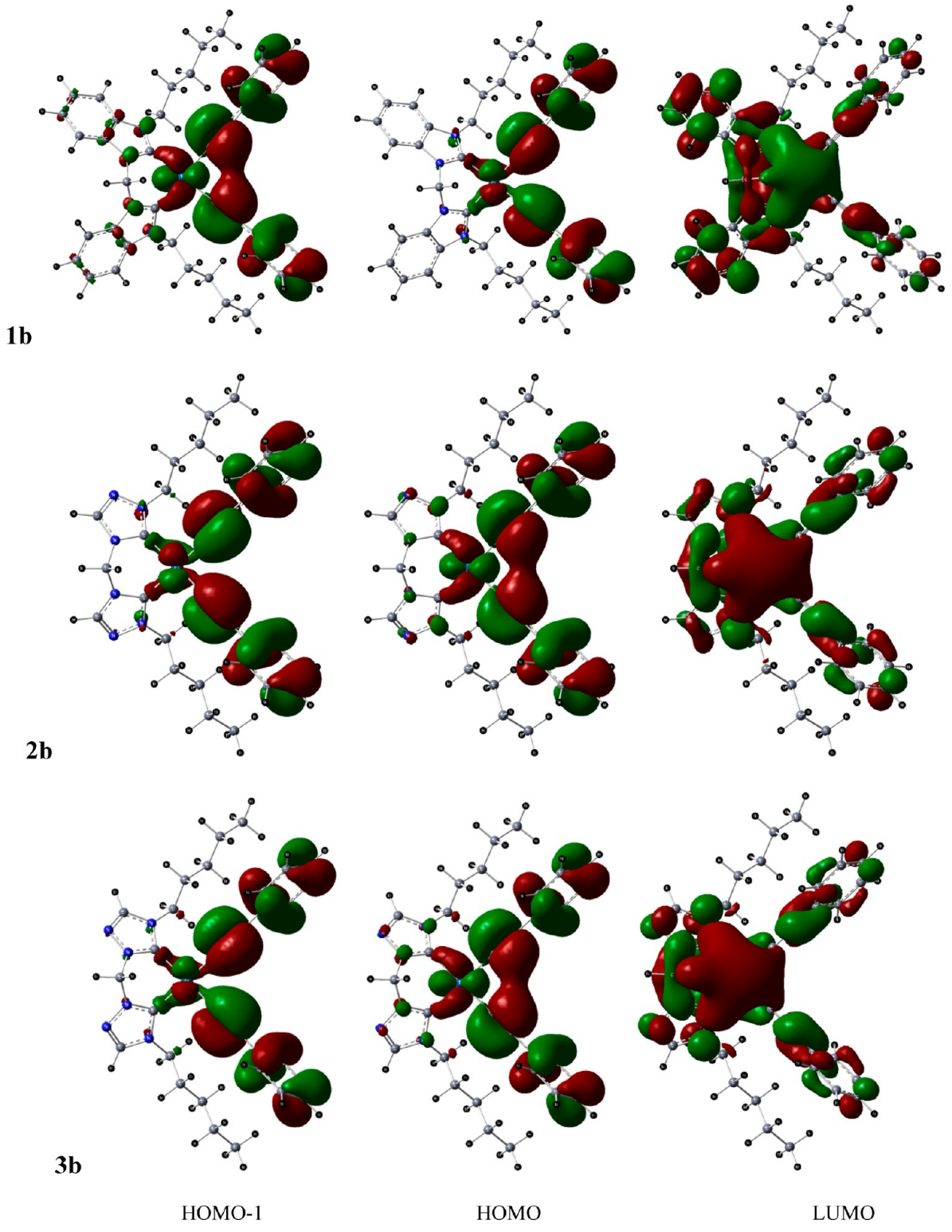

Figure 6. Spatial plots of selected frontier orbitals of the optimized ground states of **1b**−**3b**.

pyridine ligand. The spin density plots, which take into account the electron density on all α and β singly occupied orbitals of the triplet states, confirm the assumptions described above and visually identify the phosphorescence of our molecules (Figure 8). The emitting states of compounds **1b**−**3b** are very similar showing ^{3}ILCT($\pi_{alk} \rightarrow \pi^*_{alk}$) and ^{3}MLCT(Pt $\rightarrow \pi^*_{alk}$) characters, while the presence of the pyridine ligand in **4b**−**5b** reduces the contribution of the metal center and increases the participation of the N-heterocyclic carbene ligands through metal-perturbed ^{3}LLCT($\pi_{pyr} \rightarrow \pi^*_{alk}$) and ^{3}ILCT($\pi_{alk} \rightarrow \pi^*_{alk}$) characters (Tables 5 − 6).

■ CONCLUSIONS

This Article reports the influence of the different electronic properties of the chelated NHC ligands on the luminescent quantum yields of Pt(II) bisacetylide complexes. For this

dx.doi.org/10.1021/ic401841n | *Inorg. Chem.* 2014, 53, 756−771

Table 5. Frontier Orbitals of the DFT Optimized Ground State S_0 and Triplet State T_1 Structures of 1b−3b: Energy Levels and Compositions

			1b composition (%)				**2b** composition (%)				**3b** composition (%)		
	MO	energy (eV)	carbene	alkynes	Pt	energy (eV)	carbene	alkynes	Pt	energy (eV)	carbene	alkynes	Pt
ground state	L + 2	−0.57	36	60	5	−0.45	29	64	7	−0.49	18	80	2
	L + 1	−0.92	94	4	3	−0.48	3	94	3	−0.51	10	86	4
	LUMO	−1.51	62	18	20	−1.35	42	30	28	−1.34	42	30	28
	HOMO	−5.83	2	91	7	−5.90	3	84	13	−5.90	3	84	13
	H − 1	−5.83	7	79	14	−5.91	1	94	5	−5.93	2	94	4
	H − 2	−6.42	7	72	21	−6.51	4	74	22	−6.50	4	72	24
	H − 3	−6.49	16	53	31	−6.62	10	58	32	−6.64	9	58	34
triplet state	α-HOMO	−3.05	13	73 + 2	12	−3.14	9	79 + 1	11	−3.15	8	80 + 1	11
	spin densities[a]		6	76 + 3	15		3	81 + 3	13		2	82 + 4	12

[a]Sum of Mulliken spin densities per fragment (given in %).

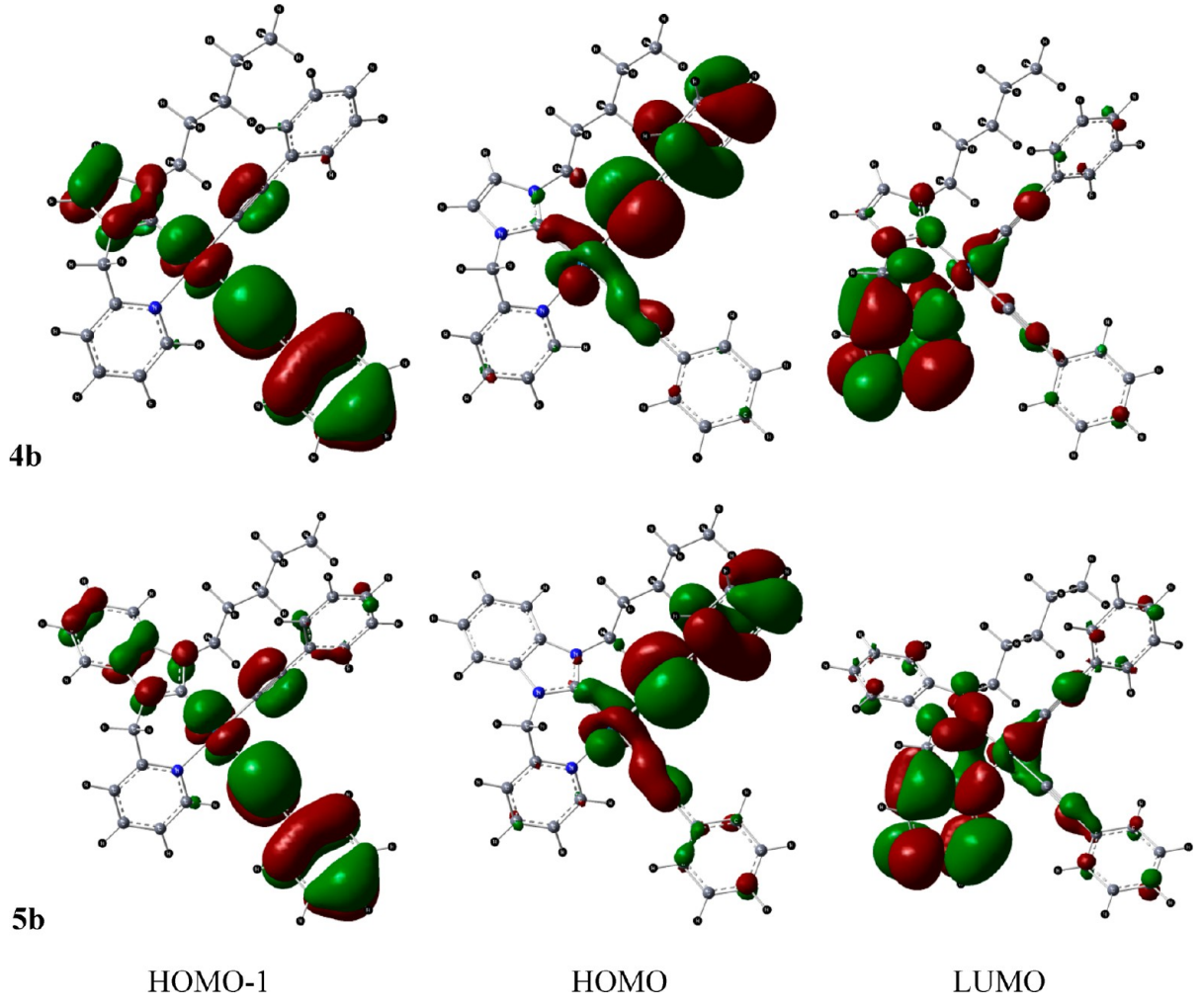

Figure 7. Spatial plots of selected frontier orbitals of the optimized ground states of **4b**− **5b**.

purpose, five new groups of complexes were prepared. Structural, electrochemical, and detailed photophysical investigations of the new complexes were carried out along with DFT and TD-DFT calculations. Most of the newly synthesized complexes displayed deep blue emission in the solid state with varying emission efficiencies that were found to be influenced by the electronic nature of the NHC and alkynyl ligands. The nature of the emission is ascribed to originate from predominantly metal perturbed ^{3}LLCT($\pi_{alk} \rightarrow \pi^*_{alk}$) in the case of the bis NHC complexes and an admixture of metal perturbed ^{3}LLCT($\pi_{alk} \rightarrow \pi^*_{alk}$) and ^{3}MLCT (Pt $\rightarrow \pi^*_{alk}$) in the complexes bearing pyridyl-NHC ligands. The results from the studies suggest a moderate electronic influence of the bis NHC ligands on the emission quantum yields and a strong influence exerted by the pyridyl NHC ligand. The resulting photophysical behaviors of the complexes are strongly suggestive of the significant impact the electronic properties of the NHC ligands bear on the excited states of the Pt(II) acetylide complexes. This work provides a further impetus to

dx.doi.org/10.1021/ic401841n | Inorg. Chem. 2014, 53, 756−771

Table 6. Frontier Orbitals of the DFT Optimized Ground State S_0 and Triplet State T_1 Structures of 4b and 5b: Energy Levels and Compositions

			4b composition (%)						5b composition (%)				
	MO	energy (eV)	carb	pyr	alk_{carb}	alk_{pyr}	Pt	energy (eV)	carb	pyr	alk_{carb}	alk_{pyr}	Pt
ground state	L + 2	−0.84	3	45	39	3	8	−0.94	2	90	0	2	1
	L + 1	−0.99	5	57	19	1	12	−1.21	49	20	17	0	11
	LUMO	−1.71	2	84	4	1	7	−1.76	8	72	6	0	9
	HOMO	−5.80	1	1	2	83	14	−5.83	0	1	4	82	13
	H − 1	−5.85	9	0	70	3	18	−5.92	8	0	70	5	17
	H − 2	−6.42	2	3	4	56	35	−6.48	2	3	4	57	34
	H − 3	−6.66	3	4	71	9	13	−6.70	1	5	72	9	14
triplet state	α-HOMO	−2.94	5	19	64	0	12	−3.02	8	11	67	0	12
	spin densities[a]		1	11	71	1	16		0	8	73	2	17

[a]Sum of Mulliken spin densities per fragment (given in %).

the development of highly efficient deep blue emitters based on Pt(II) acetylide complexes with novel chelating NHC ligands.

EXPERIMENTAL SECTION

General Procedure. All manipulations requiring inert atmosphere were carried out using standard Schlenk techniques under dinitrogen. ^{1}H, ^{13}C{^{1}H}, and ^{19}F NMR spectra were recorded on Bruker 400 and 500 MHz or Varian 200 and 300 MHz spectrometers. Chemical shifts (δ) are reported in parts per million (ppm) referenced to tetramethylsilane (δ 0.00) ppm using the residual protio solvent peaks as internal standards (^{1}H NMR experiments) or the characteristic resonances of the solvent nuclei (^{13}C NMR experiments). ^{19}F NMR was referenced to $CFCl_3$ (δ 0.00) ppm. Coupling constants (J) are quoted in Hertz (Hz), and the following abbreviations are used to describe the signal multiplicities: s (singlet); d (doublet); t (triplet); q (quartet); m (multiplet). Proton and carbon assignments have been made using routine one- and two-dimensional NMR spectroscopies where appropriate. Infrared (IR) spectra were recorded on a Perkin-Elmer 1600 Fourier transform spectrophotometer using KBr pellet with frequencies (ν_{max}) quoted in wavenumbers (cm^{-1}). Elemental microanalysis was carried out with a Leco CHNS-932 analyzer. Mass spectra were run on a Finnigan-MAT-8400 mass spectrometer. TLC analysis was performed on precoated Merck Silica Gel60F254 slides and visualized by luminescence quenching either at (short wavelength) 254 nm or (long wavelength) 365 nm. Chromatographic purification of products was performed on a short column (length 15.0 cm, diameter 1.5 cm) using silica gel 60, 230−400 mesh using a forced flow of eluent. UV−vis absorption measurements were carried out on a Perkin-Elmer Lambda 19 UV−vis spectrophotometer. Emission spectra were acquired on Perkin-Elmer spectrophotometer using 450 W xenon lamp excitation by exciting at the longest-wavelength absorption maxima with the excitation slit width 5 nm and emission slit width 10 nm. All samples for emission spectra were degassed by at least three freeze−pump−thaw cycles in an anaerobic cuvette and were pressurized with N_2 following each cycle. The 77 K emission spectra were acquired in frozen 2-methyltetrahydrofuran (2-MeTHF) glass. Luminescence quantum yields ϕ_{em} of the complexes in solution were determined at 298 K (estimated uncertainty ±15%) using standard methods, and wavelength-integrated intensities (I) of the corrected emission spectra were compared to isoabsorptive spectra of quinine sulfate standard (ϕ_{ref} = 0.55 in 1 N H_2SO_4 air-equilibrated solution) and were corrected for solvent refractive index. Absolute quantum yields were measured in neat solid and thin films using an integrating sphere on the Edinburgh spectrophotometer FLS920. YAG:Ce (powder) was used as a calibration reference with ϕ_{em} = 97%. Phosphorescent lifetimes in thin films were measured on the Edinburgh laser flash photolysis spectrophotometer LP920 with a Nd:YAG 355 nm laser as an excitation source fitted with a single monochromator. Cyclic voltamograms were measured with a Methrom 757 VA Computrace with a glassy carbon electrode (d = 2 mm) or a gold electrode with a Pt counter electrode versus Ag/AgCl reference electrode.

All starting materials were purchased from commercial sources and used as received unless stated otherwise. The solvents used for synthesis were of analytical grade. The ligands 1,1′-dipentyl-3,3′-methylene-dibenzolimidazolium diiodide [**pmdb**H_2]I_2,[9b] 1,1′-dipentyl-3,3′-methylene-di-1,2,4-triazolium dibromide [**pm2tz**H_2]Br_2,[9b] and 1,1′-dipentyl-3,3′-methylene-di-1,3,4-triazolium diiodide [**pm3tz**H_2]-I_2,[22] and precursors bis(*N*-pentyl-*N*′-picolylimidazolin-2-ylidene)silver dibromoargentate [(**ppim**)$_2$Ag]·[$AgBr_2$] and bis(*N*-pentyl-*N*′-picolyl-benzimidazolin-2-ylidene)silver dibromoargentate [(**ppbim**)$_2$Ag]·[$AgBr_2$], were synthesized by reported procedures.[10]

[pmdbH_2]I_2. 1-Pentylbenzimidazole (2.14 g, 11.37 mmol) dissolved in 5 mL of THF was mixed with methylene iodide (1.52 g, 0.46 mL, 5.68 mmol), and the mixture was heated at 110 °C for 3 days in an autoclave. The resulting product was washed with cold THF (5 times) to give a yellow solid. Yield: 1.17 g, 32%. ^{1}H NMR (300 MHz, d_6-DMSO, 300 K): δ (ppm) = 10.25 (s, 2H, NC*H*N), 8.37 (m, 2H, benzimidazole), 8.17 (m, 2H, benzimidazole), 7.78 (m, 4H, benzimidazole), 7.36 (s, 2H, NCH_2N), 4.56 (m, 4H, NCH_2CH$_2$), 1.91 (m, 4H, NCH$_2$CH_2), 1.33 (m, 8H, CH_2CH_2CH_2CH$_3$), 0.87 (m, 6H, CH$_2$CH_3). ^{13}C{^{1}H} NMR (125.8 MHz, CD_2Cl_2, 300 K): 143.7, 143.6, 131.1, 130.5, 127.5, 127.2, 124.2, 113.6, 55.2, 47.3, 28.1, 27.8, 21.7, 13.8. ESI$^+$ MS m/z: 517.2 [M − I]$^+$ (M = $C_{25}H_{34}I_2N_4$). Anal. Calcd for $C_{25}H_{34}I_2N_4$: C, 46.60; H, 5.32; N, 8.69. Found: C, 46.31; H, 5.48; N, 8.41.

[pm2tzH_2]Br_2. The procedure was adopted similar to that for [pmdbH_2]I_2. A white compound was obtained. Yield: 46%. ^{1}H NMR (500 MHz, CD_2Cl_2, 300 K): δ (ppm) = 11.72 (s, 2H, triazole), 10.35 (s, 2H, triazole), 7.94 (s, 2H, NCH_2N), 4.47 (m, 4H, NCH_2CH$_2$), 2.06 (m, 4H, NCH$_2$CH_2), 1.44 (m, 8H, CH_2CH_2CH_2CH$_3$), 0.91 (m, 6H, CH_3). ^{13}C{^{1}H} NMR (125.8 MHz, CD_2Cl_2, 300 K): 145.2, 144.2 (C of triazole), 55.9 (NCH_2N), 53.8, 28.8, 28.6, 22.6, 14.1 (C of (CH_2)$_4$CH$_3$). Anal. Calcd for $C_{15}H_{28}Br_2N_6$·0.2 H_2O: C, 39.45; H, 6.29; N, 18.40. Found: C, 39.54; H, 6.22; N, 18.09.

[Pt(pmdb)I_2] (I) . [pmdbH_2]I_2 (1.01 g, 1.57 mmol) dissolved in DMSO (20 mL) was added to platinum(II) acetylacetonate (0.62 g, 1.57 mmol) dissolved in DMSO (20 mL) at 100 °C over 18 h by a syringe pump. The reaction mixture was stirred at 110 °C for an additional 2 h after completion of addition. After removing solvent *in vacuo*, the resulting product was purified by column chromatography over silica gel using acetone/hexane (v/v 1:2) as the eluent. The pure product was isolated as white powder. Yield: 565 mg, 43%. ^{1}H NMR (500 MHz, CD_2Cl_2, 300 K): δ (ppm) = 7.30 (d, 2H, ^3J = 10.0 Hz, benzimidazole), 7.19 (d, 2H, ^3J = 10.0 Hz, benzimidazole), 7.10 (dt, 4H, benzimidazole), 6.38 (d, 1H, ^2J = 15.0 Hz, NC*H*HN), 6.03 (d, 1H, ^2J = 15.0 Hz, NCH*H*N), 4.91 (m, 2H, NC*H*HCH$_2$), 4.05 (m, 2H, NCH*H*CH$_2$), 1.65 (m, 4H, NCH$_2$CH_2), 1.12 (m, 8H, CH_2CH_2CH$_3$), 0.73 (t, 6H, CH$_2$CH_3). ^{13}C{^{1}H} NMR (125.8 MHz, CD_2Cl_2, 300 K): 162.3 (C═Pt), 134.1, 132.3, 124.4, 124.2, 112.6, 110.8 (C on benzimidazole), 57.6 (NCH_2N), 50.1, 29.6, 29.3, 23.4, 14.6 (C on (CH$_2$)$_4$CH$_3$). ESI$^+$ MS m/z: 860.0 [M + Na]$^+$ (M = $C_{25}H_{32}I_2N_4Pt$).

dx.doi.org/10.1021/ic401841n | Inorg. Chem. 2014, 53, 756−771

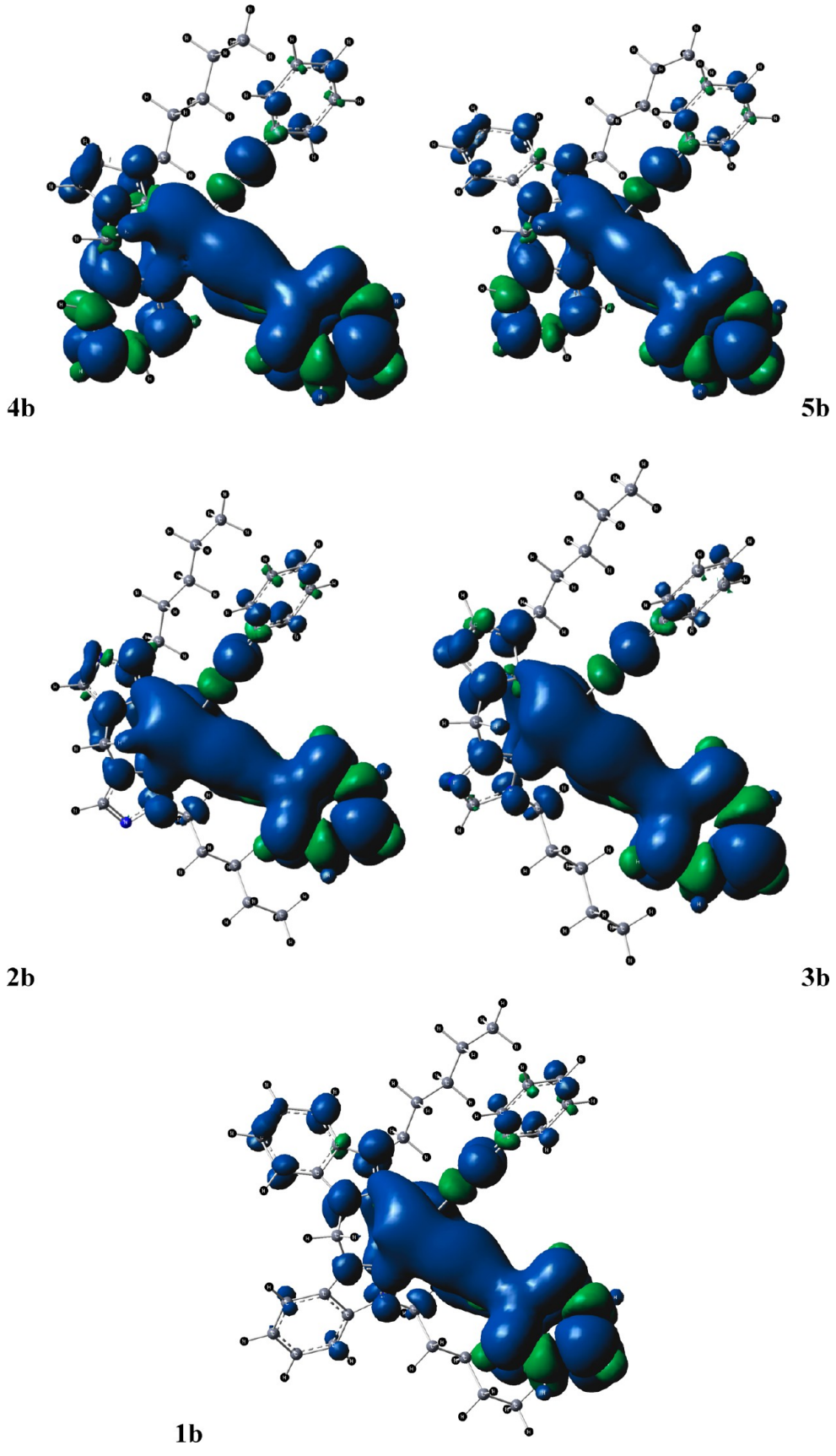

Figure 8. Spin density surfaces for the optimized triplet states of **1b**−**5b** (the positive spin densities are shown in blue and the negative ones are in green).

dx.doi.org/10.1021/ic401841n | *Inorg. Chem.* 2014, 53, 756−771

Anal. Calcd for $C_{25}H_{32}I_2N_4Pt$: C, 35.86; H, 3.85; N, 6.69. Found: C, 36.14; H, 3.87; N, 6.59. IR (cm^{-1}): 2955.07, 2928.53, 1423.90, 1391.27, 747.74.

[Pt(pm2tz)Br$_2$] (II). Platinum(II) acetylacetonate (1.39 g, 3.25 mmol) was dissolved in DMSO (20 mL) and heated to 100 °C. [pm2tzH$_2$]Br$_2$ (1.63 g, 3.25 mmol) dissolved in DMSO (20 mL) was added over 18 h with a syringe pump. The reaction solution was stirred at 100 °C additionally for another 2 h. After removing solvent *in vacuo*, the resulting product was purified by washing twice with water and twice with MeOH. The pure compound was isolated as white powder. Yield: 1.71 g, 82%. ^{1}H NMR (500 MHz, d_6-DMSO, 300 K): δ (ppm) = 8.79 (s, 2H, triazole), 6.40 (d, 1H, ^2J = 15.0 Hz, NC*H*HN), 6.07 (d, 1H, ^2J = 15.0 Hz, NCH*H*N), 4.75 (m, 2H, NC*H*HCH$_2$), 4.30 (m, 2H, NCH*H*CH$_2$), 1.80 (m, 4H, NCH$_2$C*H*$_2$), 1.20 (m, 8H, C*H*$_2$C*H*$_2$CH$_3$), 0.83 (t, 6H, CH$_2$C*H*$_3$). ^{13}C{^{1}H} NMR (125.8 MHz, d_6-DMSO, 300 K): 147.5 (*C*═Pt), 142.7 (C on triazole), 58.6 (NCH$_2$N), 51.8, 28.7, 27.7, 21.5, 13.7 (C on (CH$_2$)$_4$CH$_3$). Anal. Calcd for $C_{15}H_{26}Br_2N_6Pt$: C, 27.92; H, 4.06; N, 13.02. Found: C, 27.84; H, 4.05; N, 12.88. IR (ATR, cm^{-1}): 2957, 2860, 1617, 1467, 1358, 823.

[Pt(pm3tz)I$_2$] (III). Platinum(II) acetylacetonate (0.72 g, 1.83 mmol) was dissolved in DMSO (5 mL) and heated to 100 °C. [pm3tzH$_2$]I$_2$ (1.00 g, 1.83 mmol) dissolved in DMSO (20 mL) was added over 18 h with a syringe pump. The reaction mixture was stirred at 100 °C for another 2 h. After removal of the solvent *in vacuo*, the resulting product was purified by column chromatography using DCM/EtOAc (v/v 19:1) as the eluent. Yield: 309 mg, 22%. ^{1}H NMR (400 MHz; CD$_2$Cl$_2$, 300 K): δ (ppm) = 8.05 (s, 2H, triazole), 6.53 (d, 1H, ^2J = 16.0 Hz, NC*H*HN), 6.07 (d, 1H, ^2J = 16.0 Hz, NCH*H*N), 4.95 (m, 2H, NC*H*HCH$_2$), 4.23 (m, 2H, NCH*H*CH$_2$), 1.95 (m, 4H, NCH$_2$C*H*$_2$), 1.38 (m, 8H, C*H*$_2$C*H*$_2$CH$_3$), 0.94 (t, 6H, CH$_2$C*H*$_3$). ^{13}C{^{1}H} NMR (100.6 MHz, CD$_2$Cl$_2$, 300 K): 155.6 (*C*═Pt), 143.2 (C on triazole), 66.2 (NCH$_2$N), 50.3, 29.8, 28.3, 22.1, 13.6 (C of (CH$_2$)$_4$CH$_3$). ESI$^+$ MS *m*/*z*: 612.2 [M − I]$^+$ (M = $C_{15}H_{26}N_6I_2Pt$). Anal. Calcd for $C_{15}H_{26}N_6I_2Pt$: C, 24.37; H, 3.54; N, 11.37. Found: C, 24.21; H, 3.43; N, 11.20. IR (ATR, cm^{-1}): 2955.3, 2929.1, 1618.9, 1535.4, 1461.9, 820.1.

General Procedure for the Synthesis of 1a−c, 2a−c, and 3a−c. A 2.1 equiv portion of the acetylene ligand was dissolved in dry diethyl ether (20 mL) and cooled to −78 °C. A 2 equiv portion of *n*-butyllithium (1.6 M in hexane) was added and stirred for 30 min at −78 °C, and the temperature of the reaction was raised to −30 °C and stirred at this temperature for 30 min. Then the solution was transferred to a Schlenk flask containing the precursor suspended in dry ether at −78 °C. The mixture was then heated to 45 °C and stirred additionally for another 4 h. The reaction was quenched with water and washed with brine. The organic layer was separated, and the aqueous layer was extracted three times with dichloromethane (15 mL). The organic layer was separated, dried over MgSO$_4$, and concentrated *in vacuo*. The resulting product was purified by column chromatography over silica gel with a suitable eluent.

[Pt(pmdb)(C≡CC$_6$H$_4$F)$_2$], ***1a.*** A light yellow compound was obtained. Eluent: acetone/hexane (v/v 1:3.5). Yield: 61%. ^{1}H NMR (400 MHz, CD$_2$Cl$_2$, 300 K): δ (ppm) = 7.61 (d, 2H, ^3J = 7.47 Hz, benzimidazole), 7.54 (d, 2H, ^3J = 7.6 Hz, benzimidazole), 7.42−7.31 (m, 4H, benzimidazole, 4H, phenyl), 6.91 (t, 4H, ^3J = 8.8 Hz, phenyl), 6.98 (quart., 2H, ^2J = 13.4, NC*H*$_2$N), 5.48−5.41 (m, 2H, NC*H*HCH$_2$), 4.48−4.41 (m, 2H, NCH*H*CH$_2$), 1.96−1.88 (m, 4H, NCH$_2$C*H*$_2$), 1.40−1.18 (m, 8H, C*H*$_2$C*H*$_2$CH$_3$), 0.80 (t, 6H, ^3J = 6.8 Hz, CH$_2$C*H*$_3$). ^{13}C{^{1}H} NMR (100.6 MHz, CD$_2$Cl$_2$, 300 K): 178.5 (*C*═Pt), 161.0 (d, $^1J_{F-C}$ = 243.6 Hz), 134.7, 133.0, 125.2, 124.2, 124.1, 115.1, 114.9, 112.1, 109.6 (C on benzimidazole), 108.4, 104.6 (Pt—*C*≡*C*), 56.5 (NCH$_2$N), 48.3, 30.1, 29.4, 22.8, 14.1 (C on (CH$_2$)$_4$CH$_3$). ^{19}F NMR (188.3 MHz, CD$_2$Cl$_2$, 300 K): δ (ppm) = −117.2. Anal. Calcd for $C_{41}H_{40}F_2N_4Pt$: C, 59.92; H, 4.91; N, 6.82. Found: C, 59.82; H, 4.88; N, 6.78. IR (ATR, cm^{-1}) ν(C≡C) = 2103.

[Pt(pmdb)(C≡CC$_6$H$_5$)$_2$], ***1b.*** A light yellow compound was obtained. Eluent: acetone/hexane (v/v 1:3.5). Yield: 56%. ^{1}H NMR (400 MHz, CD$_2$Cl$_2$, 300 K): δ (ppm) = 7.62 (d, 2H, ^3J = 7.6 Hz, benzimidazole), 7.44 (d, 2H, ^3J = 7.8 Hz, benzimidazole), 7.39−7.31 (m, 4H, benzimidazole, 4H, phenyl), 7.22 (t, 4H, ^3J = 7.6 Hz, phenyl), 7.11 (t, 2H, ^3J = 7.6 Hz, phenyl), 6.48 (quart., 2H, ^2J = 13.2 Hz, NC*H*$_2$N), 5.58−5.51 (m, 2H, NC*H*HCH$_2$), 4.44−4.37 (m, 2H, NCH*H*CH$_2$), 1.96−1.88 (m, 4H, NCH$_2$C*H*$_2$), 1.44−1.18 (m, 8H, C*H*$_2$C*H*$_2$CH$_3$), 0.81 (t, 6H, ^3J = 7.2 Hz, CH$_2$C*H*$_3$). ^{13}C{^{1}H} NMR (100.6 MHz, CD$_2$Cl$_2$, 300 K): 178.7 (*C*═Pt), 134.8, 133.3, 131.7, 129.3, 128.4, 125.5, 124.2 (C on phenyl), 112.2, 109.4 (C on benzimidazole), 105.8 (Pt—*C*≡*C*), 56.9 (NCH$_2$N), 48.4, 30.3, 29.6, 22.9, 14.3 (C on (CH$_2$)$_4$CH$_3$). Anal. Calcd for $C_{41}H_{42}N_4Pt$: C, 62.66; H, 5.39; N, 7.13. Found: C, 62.81; H, 5.56; N, 6.95. IR (ATR, cm^{-1}) ν(C≡C) = 2105.

[Pt(pmdb)(C≡CC$_6$H$_4$OCH$_3$)$_2$], ***1c.*** A light yellow compound was obtained. Eluent: ether acetate/DCM (v/v 2:18). Yield: 79%. ^{1}H NMR (500 MHz, CD$_2$Cl$_2$, 300 K): δ (ppm) = 7.60 (d, 2H, ^3J = 8.0 Hz, benzimidazole), 7.46 (d, 2H, ^3J = 8.0 Hz, benzimidazole), 7.41−7.33 (m, 4H, benzimidazole), 7.30 (d, 4H, ^3J = 9.0 Hz, phenyl), 6.77 (d, 4H, ^3J = 10.0 Hz, phenyl), 6.45 (q, 2H, ^2J = 13.5 Hz, NC*H*$_2$N), 5.59−5.53 (m, 2H, NC*H*HCH$_2$), 4.44−4.38 (m, 2H, NCH*H*CH$_2$), 3.77 (s, 6H, OC*H*$_3$), 1.97−1.87 (m, 4H, NCH$_2$C*H*$_2$), 1.40−1.19 (m, 8H, C*H*$_2$C*H*$_2$CH$_3$), 0.81 (t, 6H, ^3J = 7.0 Hz, CH$_2$C*H*$_3$). ^{13}C{^{1}H} NMR (125.8 MHz, CD$_2$Cl$_2$, 300 K): 179.0 (C═Pt), 157.9, 134.9, 133.3, 132.8, 124.2, 124.1, 122.2, 121.9, 113.9 (C on phenyl), 112.2, 109.8 (C on benzimidazole), 109.4, 103.1 (Pt-*C*≡*C*), 100.1, 56.8 (NCH$_2$N), 55.7, 48.4, 30.3, 29.6, 23.0, 14.3 (C on (CH$_2$)$_4$CH$_3$). Anal. Calcd for $C_{43}H_{46}N_4O_2Pt$: C, 61.05; H, 5.48; N, 6.62. Found: C, 61.14; H, 5.46; N, 6.55. IR (ATR, cm^{-1}) ν(C≡C) = 2105.

[Pt(pm2tz)(C≡CC$_6$H$_4$F)$_2$], ***2a.*** A light yellow compound was obtained. Eluent: acetone/hexane (v/v 1:2). Yield: 51%. ^{1}H NMR (500 MHz, CD$_2$Cl$_2$, 300 K): δ (ppm) = 8.26 (s, 2H, triazole), 7.25 (t, 4H, ^3J = 8.0 Hz, phenyl), 6.90 (t, 4H, ^3J = 8.0 Hz, phenyl), 6.19 (s, 2H, NC*H*$_2$N), 4.96−4.53 (m, 4H, NC*H*$_2$CH$_2$), 1.88 (s, 4H, NCH$_2$C*H*$_2$), 1.22−1.15 (m, 8H, C*H*$_2$C*H*$_2$CH$_3$), 0.78 (t, 6H, ^3J = 6.5 Hz C*H*$_3$). ^{13}C{^{1}H} NMR (125.8 MHz, CD$_2$Cl$_2$, 300 K), δ (ppm) = 167.7 (Pt═*C*), 162.0 (C $^1J_{F-C}$ = 240 Hz, C−F), 140.4 (C on triazole), 133.1, 132.4, 124.0, 115.4, 115.3, 114.8 (C on the phenyl), 108.0, 102.4 (Pt—*C*≡*C*), 58.7 (C on NCH$_2$N), 52.7, 30.4, 29.2, 28.9, 28.6, 22.9, 14.2 (C on (CH$_2$)$_4$CH$_3$). ^{19}F NMR (188.3 MHz, CD$_2$Cl$_2$, 300 K): δ (ppm) = −116.2. ESI$^+$ MS *m*/*z*: 724.2 [M]$^+$ (M = $C_{31}H_{34}F_2N_6Pt$). Anal. Calcd for $C_{31}H_{34}F_2N_6Pt$: C, 51.45; H, 4.74; N, 11.61. Found: C, 51.31; H, 4.74; N, 11.45. IR (ATR, cm^{-1}) ν(C≡C) = 2109.

[Pt(pm2tz)(C≡CC$_6$H$_4$)$_2$], ***2b.*** A light yellow compound was obtained. Eluent: DCM/EtOAc (v/v 19:1). Yield: 60%. ^{1}H NMR (400 MHz, CD$_2$Cl$_2$, 300 K): δ (ppm) = 8.26 (s, 2H, triazole), 7.27 (d, 4H, ^3J = 8.0 Hz, phenyl), 7.20 (t, 4H, ^3J = 7.6 Hz, phenyl), 7.12 (t, 2H, ^3J = 6.8 Hz, phenyl), 6.20 (s, 2H, NC*H*$_2$N), 4.91−4.59 (m, 4H, NC*H*$_2$CH$_2$), 1.92−1.84 (m, 4H, NCH$_2$C*H*$_2$), 1.26−1.18 (m, 8H, C*H*$_2$C*H*$_2$CH$_3$), 0.78 (t, 6H, ^3J = 6.8 Hz, C*H*$_3$). ^{13}C{^{1}H} NMR (100.6 MHz, CD$_2$Cl$_2$, 300 K), δ (ppm) = 168.7 (Pt═*C*), 140.6 (C on triazole), 131.6, 128.7, 128.5, 125.9 (C on the phenyl), 109.7, 103.9 (Pt-*C*≡*C*), 59.1 (C on NCH$_2$N) 30.3, 29.2, 22.9, 14.2 (C on (CH$_2$)$_4$CH$_3$). ESI$^+$ MS *m*/*z*: 688.3 [M]$^+$ (M = $C_{31}H_{36}N_6Pt$). Anal. Calcd for $C_{31}H_{36}N_6Pt$: C, 54.10; H, 5.28; N, 12.22. Found: C, 53.98; H, 5.32; N, 12.09. IR (ATR, cm^{-1}) ν(C≡C) = 2110.

[Pt(pm2tz)(C≡CC$_6$H$_4$OCH$_3$)$_2$], ***2c.*** A white compound was obtained. Eluent: acetone/hexane (v/v 1:2). Yield: 21%. ^{1}H NMR (500 MHz, CD$_2$Cl$_2$, 300 K): δ (ppm) = 8.49 (s, 2H, triazole), 7.16 (d, 4H, ^3J = 10.0 Hz, phenyl), 6.74 (t, 4H, ^3J = 10.0 Hz, phenyl), 5.32 (s, 2H, NC*H*$_2$N), 4.89−4.56 (m, 4H, NC*H*$_2$CH$_2$), 3.74 (s, 6H, OC*H*$_3$), 1.95−1.80 (m, 4H, NCH$_2$C*H*$_2$), 1.24−1.16 (m, 8H, C*H*$_2$C*H*$_2$CH$_3$), 0.78 (t, 6H, ^3J = 6.5 Hz C*H*$_3$). ^{13}C{^{1}H} NMR (125.8 MHz, CD$_2$Cl$_2$, 300 K), δ (ppm) = 168.0 (Pt═*C*), 158.3, 141.4 (C on triazole), 132.4, 120.8, 114.3, (C on the phenyl), 109.7, 101.8 (Pt—*C*≡*C*), 59.4 (C on NCH$_2$N), 55.7 (OCH$_3$), 53.1, 30.4, 29.9, 29.2, 29.0, 22.8, 14.3 (C of (CH$_2$)$_4$CH$_3$). ESI$^+$ MS *m*/*z*: 749.2 [M]$^+$ (M = $C_{33}H_{40}N_6O_2Pt$). $C_{33}H_{40}N_6O_2Pt$: C, 53.00; H, 5.39; N, 11.24. Found: C, 52.86; H, 5.65; N, 11.21. IR (ATR, cm^{-1}) ν(C≡C) = 2113.

[Pt(pm2tz)(C≡CSi(CH$_3$)$_3$)$_2$], ***2d.*** A white compound was obtained after washing twice with pentane. Single crystal was obtained from the slow evaporation of dichloromethane and methanol. Yield: 18%. ^{1}H NMR (400 MHz, CD$_2$Cl$_2$, 300 K): δ (ppm) = 8.68 (s, 2H, triazole),

dx.doi.org/10.1021/ic401841n | *Inorg. Chem.* 2014, 53, 756−771

7.26 (s, 1H, NC*H*HN), 5.82 (s, 1H, NCH*H*N), 5.43 (s, 2H, NCH*H*CH$_2$), 4.18−4.06 (m, 2H, NC*H*HCH$_2$), 1.84−1.77 (m, 4H, NCH$_2$C*H*$_2$), 1.36−1.24 (m, 8H, C*H*$_2$C*H*$_2$CH$_3$), 0.87 (t, ^3J = 7.2 Hz 6H, C*H*$_3$), −0.07 (m, 18H, Si(C*H*$_3$)$_3$). ^{13}C{^{1}H} NMR (100.6 MHz, CD$_2$Cl$_2$, 300 K): δ (ppm) = 168.2 (Pt=*C*), 141.8 (C on triazole), 125.3, 114.5 (Pt—C≡*C*), 59.2 (NCH$_2$N), 53.3 (NCH$_2$CH$_2$), 30.6, 29.1 22.9, 14.2 (C on (CH$_2$)$_4$CH$_3$) 1.1 (Si(CH$_3$)$_3$). ESI$^+$ MS *m*/*z*: 679.3 [M]$^+$ (M = $C_{25}H_{44}N_6PtSi_2$). Anal. Calcd for $C_{25}H_{44}N_6PtSi_2$: C, 44.16; H, 6.52; N, 12.36. Found: C, 44.16; H, 6.38; N, 12.16. IR (ATR, cm^{-1}) ν(C≡C) = 2035.

[Pt(pm3tz)(C≡CC$_6$H$_4$F)$_2$], ***3a***. A light yellow compound was obtained. Eluent: DCM/EtOAc (v/v 19:1). Yield: 87%. ^{1}H NMR (400 MHz, CD$_2$Cl$_2$, 300 K): δ (ppm) = 8.01 (s, 2H, triazole), 7.32−7.28 (m, 4H, phenyl), 6.92 (t, 4H, ^3J = 8.8 Hz, phenyl), 6.28 (s, 2H, NC*H*$_2$N), 4.74−4.65 (m, 4H, NC*H*$_2$CH$_2$), 1.89 (m, 4H, NCH$_2$C*H*$_2$), 1.43−1.15 (m, 8H, C*H*$_2$C*H*$_2$CH$_3$), 0.81 (t, 6H, ^3J = 8.0 Hz, C*H*$_3$). ^{13}C{^{1}H} NMR (100.6 MHz, CD$_2$Cl$_2$, 300 K): δ (ppm) = 170.4 (Pt=*C*), 161.9, 143.3 (C on triazole), 133.2, 115.4, 115.2 (C on the phenyl), 108.3, 102.0 (Pt-C≡*C*), 66.8 (C of NCH$_2$N), 49.4, 31.4, 29.2, 22.9, 14.2 (C of (CH$_2$)$_4$CH$_3$). ^{19}F NMR (376.5 MHz, CD$_2$Cl$_2$, 300 K): δ (ppm)= −116.9. Anal. Calcd for $C_{31}H_{34}F_2N_6Pt\cdot0.2CH_3C(O)OC_2H_5$: C, 51.54; H, 4.87; N, 11.27. Found: C, 51.77; H, 4.98; N, 11.08. IR (ATR, cm^{-1}) ν(C≡C) = 2117.

[Pt(pm3tz)(C≡CC$_6$H$_5$)$_2$], ***3b***. A light yellow compound was obtained. Eluent: DCM/EtOAc (v/v 19:1). Yield: 64%. ^{1}H NMR (400 MHz, CD$_2$Cl$_2$, 300 K): δ (ppm) = 8.00 (s, 2H, triazole), 7.33 (d, 4H, ^3J = 7.2 Hz, phenyl), 7.21 (t, 4H, ^3J = 8.0 Hz, phenyl), 7.11 (t, 2H, ^3J = 7.2 Hz, phenyl), 6.34 (s, 2H, NC*H*$_2$N), 4.78−4.68 (m, 4H, NC*H*$_2$CH$_2$), 1.93−1.86 (m, 4H, NCH$_2$C*H*$_2$), 1.29−1.23 (m, 8H, C*H*$_2$C*H*$_2$CH$_3$), 0.81 (t, 6H, ^3J = 7.2 Hz, C*H*$_3$). ^{13}C{^{1}H} NMR (100.6 MHz, CD$_2$Cl$_2$, 300 K): δ (ppm) = 170.4 (Pt=*C*), 143.3 (C on triazole), 131.6, 128.9, 128.4, 125.7 (C on the phenyl), 109.7, 102.8 (Pt—C≡*C*), 66.9 (C of NCH$_2$N) 49.4, 31.4, 29.2, 22.8, 14.2 (C of (CH$_2$)$_4$CH$_3$). Anal. Calcd for $C_{31}H_{36}N_6Pt$: C, 54.14; H, 5.28; N, 12.22. Found: C, 54.04; H, 5.32; N, 12.19. IR (ATR, cm^{-1}) ν(C≡C) = 2107.

[Pt(pm3tz)(C≡CC$_6$H$_4$OCH$_3$)$_2$], ***3c***. A light yellow compound was obtained. Eluent: DCM/EtOAc (v/v 18:2). Yield: 37%. ^{1}H NMR (400 MHz, CD$_2$Cl$_2$, 300 K): δ (ppm) = 7.99 (s, 2H, triazole), 7.27 (d, 4H, ^3J = 8.8 Hz, phenyl), 6.76 (t, 4H, ^3J = 8.8 Hz, phenyl), 6.27 (s, 2H, NC*H*$_2$N), 4.94 (m, 1H, NC*H*$_2$CH$_2$), 4.79−4.69 (m, 2H, NC*H*$_2$CH$_2$), 4.20−4.13 (m, 1H, NC*H*$_2$CH$_2$), 3.77 (s, 6H, OC*H*$_3$), 1.94−1.84 (m, 4H, NCH$_2$C*H*$_2$), 1.37−1.21 (m, 8H, C*H*$_2$C*H*$_2$CH$_3$), 0.82 (t, 6H, ^3J = 7.2 Hz, C*H*$_3$). ^{13}C{^{1}H} NMR (100.6 MHz, CD$_2$Cl$_2$, 300 K), δ (ppm) = 170.6 (Pt=*C*), 158.1 143.3 (C of triazole), 132.8, 121.4, 114.0, (C on the phenyl), 109.0, 100.1 (Pt—C≡*C*), 66.8 (C of NCH$_2$N), 55.7 (OCH$_3$), 49.1, 31.5, 29.4, 22.8, 14.2 (C of (CH$_2$)$_4$CH$_3$). Anal. Calcd for $C_{33}H_{40}N_6O_2Pt$: C, 53.00; H, 5.39; N, 11.24. Found: C, 53.09; H, 5.53; N, 11.19. IR (ATR, cm^{-1}) ν(C≡C) = 2109.

General Procedure for the Synthesis of 4a, 4b, 4e, 5a, 5b, and 5e. A 1 equiv portion of the silver salt was dissolved in dry DCM, added dropwise to a DCM solution of [Pt(COD)(C≡CR)$_2$], and stirred for 15 h with exclusion of light. The mixture was filtered through Celite to remove the silver salts, and the obtained residue was purified by column chromatography over silica gel with a suitable eluent.

[Pt(ppim)(C≡CC$_6$H$_4$F)$_2$], ***4a***. A light yellow compound was obtained. Eluent: Et$_2$O/EtOAc (v/v 19:1). Yield: 60%. ^{1}H NMR (400 MHz, CD$_2$Cl$_2$, 300 K): δ (ppm) = 9.62 (d, 1H, ^3J = 6.2 Hz, pyridine), 7.92 (t, 1H, ^3J = 6.8 Hz, pyridine), 7.52 (d, 1H, ^3J = 7.6 Hz, pyridine), 7.39 (dt, 1H, ^3J = 7.6 Hz, pyridine), 7.35−7.27 (m, 4H, phenyl), 7.09 (s, 1H, imidazole), 6.95 (s, 1H, imidazole), 6.94−6.89 (m, 4H, phenyl), 5.28−5.16 (m, 2H, NC*H*$_2$C), 4.60−4.49 (m, 2H, NC*H*$_2$CH$_2$), 1.88−1.81 (m, 2H, NCH$_2$C*H*$_2$), 1.55 (s, 2H, CH$_2$), 1.23−1.19 (m, 2H, C*H*$_2$CH$_3$), 0.77 (t, 3H, ^3J = 6.8 Hz, C*H*$_3$). ^{13}C{^{1}H} NMR (100.6 MHz, CD$_2$Cl$_2$, 300 K): δ (ppm) = 169.8 (Pt=*C*), 162.5 160.1 (*C*−F), 156.4, 153.4, 139.3, 133.3, 126.0 125.0 (pyridine), 120.6 (imidazole), 115.1 (phenyl), 103.0, 101.6 (*C*≡*C*), 56.3 (C of NCH$_2$N), 54.5, 31.6, 29.4, 27.5, 22.9, 14.4 (C of (CH$_2$)$_4$CH$_3$). ^{19}F NMR (188.3 MHz, CD$_2$Cl$_2$, 300 K): δ (ppm) = −116.8, −117.4. ESI$^+$ MS *m*/*z*: 663.1 [M]$^+$ (M = $C_{30}H_{27}F_2N_3Pt$). Anal. Calcd for $C_{30}H_{27}N_3F_2Pt\cdot Et_2O$: C, 55.58; H, 4.80; N, 5.72. Found: C, 55.38; H, 4.41; N, 6.00. IR (ATR, cm^{-1}) ν(C≡C) = 2121, 2106.

[Pt(ppim)(C≡CC$_6$H$_5$)$_2$], ***4b***. A light yellow compound was obtained. Eluent: DCM/EtOAc (v/v 19:1). Yield: 35%. ^{1}H NMR (400 MHz, CD$_2$Cl$_2$, 300 K): δ (ppm) = 9.66 (d, 1H, ^3J = 5.6 Hz, pyridine), 7.92 (t, 1H, ^3J = 8.0 Hz, pyridine), 7.51 (d, 1H, ^3J = 7.6 Hz, pyridine), 7.41−7.38 (m, 1H, pyridine), 7.38−7.31 (m, 4H, phenyl), 7.21 (t, 4H, ^3J = 7.6 Hz, phenyl), 7.13−7.08 (m, 2H, phenyl, 1H, imidazole), 6.95 (s, 1H, imidazole), 5.29−5.13 (m, 2H, NC*H*$_2$C), 4.64−4.5 (m, 2H, NC*H*$_2$CH$_2$), 1.89−1.81 (m, 2H, NCH$_2$C*H*$_2$), 1.27−1.19 (m, 4H, C*H*$_2$C*H*$_2$CH$_3$), 0.77 (t, 3H, ^3J = 6.8 Hz, C*H*$_3$). ^{13}C{^{1}H} NMR (100.6 MHz, CD$_2$Cl$_2$, 300 K): δ (ppm) = 169.9 (Pt=*C*), 158.3, 156.4, 139.3, 132.0, 131.8, 130.7, 129.3, 128.4, 126.0, 125.7, 125.4 (phenyl), 124.9 (pyridine), 121.1, 120.5 (imidazole), 111.0, 105.5, 104.4 (C≡C), 55.5 (C of NCH$_2$N), 51.0, 31.6, 31.2, 29.4, 22.9, 14.2 (C of (CH$_2$)$_4$CH$_3$). ESI$^+$ MS *m*/*z*: 627.3 [M]$^+$ (M = $C_{30}H_{29}N_3Pt$). Anal. Calcd for $C_{30}H_{29}N_3Pt$: C, 57.50; H, 4.66; N, 6.71. Found: C, 57.77; H, 4.72; N, 6.58. IR (ATR, cm^{-1}) ν(C≡C) = 2117, 2101.

[Pt(ppim)(C≡CC$_6$H$_4$N(C$_6$H$_5$)$_2$)$_2$], ***4e***. A brown compound was obtained. Eluent: DCM/EtOAc (v/v 19:1), slight decomposition was observed on silica gel during column chromatography. Yield: 17%. ^{1}H NMR (500 MHz, CD$_2$Cl$_2$, 300 K): δ (ppm) = 9.64 (d, 1H, ^3J = 5.6 Hz, pyridine), 7.91 (t, 1H, ^3J = 7.6 Hz, pyridine), 7.52 (d, 1H, ^3J = 7.6 Hz, pyridine), 7.38 (t, 1H, ^3J = 7.5 Hz, pyridine), 7.26 −7.19 (m, 4H, phenyl, 8H, *o*-phenyl N), 7.11 (s, 1H, imidazole), 7.06−7.04 (m, 8H, *m*-phenyl N), 7.00−6.95 (m, 4H, *p*-phenyl N), 6.94 (s, 1H, imidazole), 6.92−6.89 (m, 4H, phenyl), 5.36−5.08 (m, 2H, NC*H*$_2$C), 4.59−4.52 (m, 2H, NC*H*$_2$CH$_2$), 1.89−1.83 (m, 2H, NCH$_2$C*H*$_2$), 1.28−1.17 (m, 4H, C*H*$_2$C*H*$_2$CH$_3$), 0.78 (t, 3H, ^3J = 7.0 Hz, C*H*$_3$). ^{13}C{^{1}H} NMR (125.8 MHz, CD$_2$Cl$_2$, 300 K): δ (ppm) = 170.1 (Pt=*C*), 156.5, 153.4, 148.4, 145.6, 145.3, 139.2, 132.8, 132.6, 129.7, 126.0, 124.5, 123.1 (pyridine), 122.9, 121.0 (phenyl), 120.5 (imidazole), 115.0, 105.2, 104.1 (C≡C), 78.3, 56.9 (C of NCH$_2$N), 51.0, 31.7, 29.4, 23.0, 14.4 (C of (CH$_2$)$_4$CH$_3$). ESI$^+$ MS *m*/*z*: 960.3 [M]$^+$ (M = $C_{54}H_{47}N_5Pt$). Anal. Calcd for $C_{54}H_{47}N_5Pt$: C, 67.49; H, 4.93; N, 7.29. Found: C, 67.86; H, 4.90; N, 7.24. IR (ATR, cm^{-1}) ν(C≡C) = 2110.

[Pt(ppbim)(C≡CC$_6$H$_4$F)$_2$], ***5a***. A light yellow compound was obtained. Eluent: hexane/EtOAc (v/v 12:8). Yield: 79%. ^{1}H NMR (400 MHz, CD$_2$Cl$_2$, 300 K): δ (ppm) = 9.60 (d, 1H, ^3J = 6.8 Hz, pyridine), 7.92 (t, 1H, ^3J = 7.6 Hz, pyridine), 7.63−7.57 (m, 2H, benzimidazole), 7.49−7.47 (m, 1H, pyridine), 7.42−7.40 (m, 1H, pyridine), 7.39−7.35 (m, 4H, phenyl), 7.33−7.28 (m, 2H, benzimidazole), 6.92 (t, 4H, ^3J = 8.8 Hz, phenyl), 5.55−5.46 (m, 2H, NC*H*$_2$C), 4.99−4.79 (m, 2H, NC*H*$_2$CH$_2$), 2.00−1.93 (m, 2H, NCH$_2$C*H*$_2$), 1.34−1.27 (m, 4H, C*H*$_2$C*H*$_2$CH$_3$), 0.77 (t, 3H, ^3J = 7.2 Hz, C*H*$_3$). ^{13}C{^{1}H} NMR (100.6 MHz, CD$_2$Cl$_2$, 300 K): δ (ppm) = 179.1 (Pt=*C*), 162.6 160.1 (*C*−F), 156.3, 153.3, 139.5, 134.8, 133.7, 133.4, 126.1 125.1 (pyridine), 124.1, 115.4, 115.2 (phenyl), 112.2, 110.2 (benzimidazole), 104.3, 103.7 (*C*≡*C*), 78.2, 52.4 (C of NCH$_2$N), 48.4, 30.2, 29.7, 22.9, 14.3 (C of (CH$_2$)$_4$CH$_3$). ^{19}F NMR (188.3 MHz, CD$_2$Cl$_2$, 300 K): δ (ppm) = −117.3, −117.2. ESI$^+$ MS *m*/*z*: 761.2 [M + CHCl]$^+$ (M = $C_{34}H_{29}F_2N_3Pt$). Anal. Calcd for $C_{34}H_{29}F_2N_3Pt\cdot0.5$hexane: C, 58.80; H, 4.80; N, 5.56. Found: C, 58.81; H, 4.50; N, 5.41. IR (ATR, cm^{-1}) ν(C≡C) = 2121, 2108.

[Pt(ppbim)(C≡CC$_6$H$_5$)$_2$], ***5b***. A light yellow compound was obtained. Eluent: DCM/EtOAc (v/v 19:2). Yield: 57%. ^{1}H NMR (400 MHz, CD$_2$Cl$_2$, 300 K): δ (ppm) = 9.64 (d, 1H, ^3J = 5.6 Hz, pyridine), 7.93 (t, 1H, ^3J = 7.6 Hz, pyridine), 7.62−7.57 (m, 2H, benzimidazole), 7.48 (d, 1H,^3J = 7.6 Hz, pyridine), 7.43−7.41 (m, 1H, pyridine), 7.39−7.37 (m, 4H, phenyl), 7.35−7.33 (m, 2H benzimidazole), 7.22 (t, 4H, ^3J = 7.6 Hz, phenyl), 7.14−7.08 (m, 2H, phenyl), 5.57−5.47 (m, 2H, NC*H*$_2$C), 5.05−4.78 (m, 2H, NC*H*$_2$CH$_2$), 2.00−1.93 (m, 2H, NCH$_2$C*H*$_2$), 1.35−1.25 (m, 4H, C*H*$_2$C*H*$_2$CH$_3$), 0.77 (t, 3H, ^3J = 7.2 Hz, C*H*$_3$). ^{13}C{^{1}H} NMR (100.6 MHz, CD$_2$Cl$_2$, 300 K): δ (ppm) = 179.4 (Pt=*C*), 156.5, 153.3, 139.6, 134.9, 133.7, 132.1, 131.8, 129.2, 128.8, 128.4, 126.1, 125.8, 125.6, 125.1 (phenyl), 124.1 (pyridine), 115.7, 112.2, 110.2 (benzimidazole), 105.7, 105.1 (*C*≡*C*), 52.4 (C of NCH$_2$N), 48.3, 30.3, 29.7, 22.9, 14.3 (C of (CH$_2$)$_4$CH$_3$). ESI$^+$ MS *m*/*z*: 725.1 [M + CHCl]$^+$ (M = $C_{34}H_{31}N_3Pt$). Anal. Calcd for $C_{34}H_{31}N_3Pt$: C, 60.35; H, 4.62; N, 6.21.

dx.doi.org/10.1021/ic401841n | *Inorg. Chem.* 2014, 53, 756−771

Found: C, 60.71; H, 4.73; N, 6.03. IR (ATR, cm^{-1}) ν(C≡C) = 2121, 2106.

[Pt(ppbim)(C≡C$C_6H_4N(C_6H_5)_2$)$_2$], **5e**. A brown compound was obtained. Eluent: DCM/EtOAc (v/v 19:2), slight decomposition on silica gel during column chromatography. Yield: 25%. ^{1}H NMR (400 MHz, CD_2Cl_2, 300 K): δ (ppm) = 9.67 (d, 1H, ^3J = 6.0 Hz, pyridine), 7.92 (t, 1H, ^3J = 7.5 Hz, pyridine), 7.63−7.57 (m, 2H, benzimidazole), 7.48 (d, 1H, ^3J = 7.8 Hz, pyridine), 7.41−7.34 (m, 1H, pyridine, 2H, benzimidazole), 7.28−7.21 (m, 12H, *o*-phenyl, *m*-phenyl, N), 7.07−7.04 (m, 8H, phenyl, N), 7.01−6.96 (m, 4H, phenyl, N), 6.92 (d, 4H, ^3J = 9.0 Hz, *o*-phenyl), 5.54−5.48 (m, 2H, NCH_2C), 4.95−4.84 (m, 2H, NCH_2CH_2), 2.04−1.95 (m, 2H, NCH$_2$CH_2), 1.37−1.30 (m, 2H, CH$_2$CH_2CH$_3$), 1.25−1.18 (m, 2H, CH_2CH$_2$CH$_3$), 0.80 (t, 3H, ^3J = 7.2 Hz, CH_3). ^{13}C{^{1}H} NMR (100.6 MHz, CD_2Cl_2, 300 K): δ (ppm) = 179.3 (Pt=*C*), 156.8, 153.3, 148.3, 148.2, 145.7, 145.4, 139.4, 134.8, 133.7, 132.8, 132.6, 129.7, 129.6, 126.1, 125.0, 124.9, 124.6, 124.4 (pyridine), 124.3, 124.2, 124.0, 123.9, 123.8, 123.5, 123.1, 122.9, 114.9, 112.2, 110.16 (benzimidazole), 105.3, 104.8, 78.0, 52.3, 48.4, 30.2, 29.7, 22.9, 14.4 ((*C*H$_2$)$_4$CH$_3$). ESI$^+$ MS *m*/*z*: 1011.3 [M]$^+$ (M = $C_{58}H_{49}N_5Pt$). Anal. Calcd for $C_{58}H_{49}N_5Pt$: C, 68.90; H, 4.88; N, 6.93. Found: C, 68.89; H, 4.80; N, 6.89. IR (ATR, cm^{-1}) ν(C≡C) = 2108.

X-ray Diffraction Analyses. Single-crystal X-ray diffraction data were collected at 183(2) K on an Agilent Technologies Xcalibur Ruby area-detector diffractometer using a single wavelength Enhance X-ray source with Mo Kα radiation (λ = 0.710 73 Å)[23] from a microfocus X-ray source and an Oxford Instruments Cryojet XL cooler. The selected suitable single crystals were mounted using polybutene oil on a flexible loop fixed on a goniometer head and immediately transferred to the diffractometer. Pre-experiment, data collection, data reduction, and analytical absorption correction[24] were performed with the program suite *CrysAlisPro*.[25] Using *Olex2*,[26] the structure was solved by direct methods using *SHELXS97*[27] and refined with the *SHELXL2013*[27] program package by full-matrix least-squares minimization on F^2. *PLATON*[28] was used to check the results of the X-ray analyses. Crystal data for **I**: $C_{25}H_{32}I_2N_4Pt\cdot(CH_2Cl_2)_{0.333}\cdot(CH_4O)_{0.333}$ (*M* = 876.42), hexagonal, space group $P6_3/m$ (No. 176), *a* = 17.5075(2) Å, *c* = 16.9453(2) Å, *V* = 4498.09(12) Å^3, *Z* = 6, *T* = 183(2) K, μ(Mo Kα) = 6.819 mm^{-1}, D_{calc} = 1.941 g/mm^3, 48 697 reflections measured (5.238 ≤ 2θ ≤ 56.55), 3858 unique (R_{int} = 0.0409) which were used in all calculations. The final R1 was 0.0391 ($I > 2\sigma(I)$), and wR2 was 0.1063 (all data). Crystal data for **1a**: $C_{42}H_{46}F_2N_4PtO_2$ (*M* = 871.92), orthorhombic, space group $Pca2_1$ (No. 29), *a* = 13.7433(2) Å, *b* = 21.0614(3) Å, *c* = 13.185 80(10) Å, *V* = 3816.67(8) Å^3, *Z* = 4, *T* = 183(2) K, μ(Mo Kα) = 3.727 mm^{-1}, D_{calc} = 1.517 g/mm^3, 34 854 reflections measured (5.77 ≤ 2θ ≤ 56.562), 9470 unique (R_{int} = 0.0498) which were used in all calculations. The final R1 was 0.0347 ($I > 2\sigma(I)$), and wR2 was 0.0653 (all data). Crystal data for **1b**: $C_{85}H_{91}N_8Pt_2Cl$ (*M* = 1650.28), monoclinic, space group $P2_1/c$ (No. 14), *a* = 16.9885(7) Å, *b* = 25.6500(8) Å, *c* = 19.5345(9) Å, β = 114.494(5)°, *V* = 7746.2(6) Å^3, *Z* = 4, *T* = 183(2) K, μ(Mo Kα) = 3.691 mm^{-1}, D_{calc} = 1.415 g/mm^3, 60 100 reflections measured (5.468 ≤ 2θ ≤ 52.744), 15 828 unique (R_{int} = 0.0863) which were used in all calculations. The final R1 was 0.0701 ($I > 2\sigma(I)$), and wR2 was 0.1628 (all data). Crystal data for **2a**: $C_{65}H_{80}N_{12}F_4Pt_2O_3$ (*M* = 1543.59), triclinic, space group $P\bar{1}$ (No. 2), *a* = 13.8528(6) Å, *b* = 15.5714(5) Å, *c* = 17.8630(6) Å, α = 82.817(3)°, β = 69.071(4)°, γ = 73.626(3)°, *V* = 3451.7(2) Å^3, *Z* = 2, *T* = 183(2) K, μ(Mo Kα) = 4.110 mm^{-1}, D_{calc} = 1.485 g/mm^3, 34 609 reflections measured (5.086 ≤ 2θ ≤ 50.7), 12 649 unique (R_{int} = 0.0646) which were used in all calculations. The final R1 was 0.0539 ($I > 2\sigma(I)$), and wR2 was 0.1247 (all data). For more details about the data collection and refinements parameters, see the crystallographic information files (Supporting Information). CCDC-950233 (for **I**), CCDC-950234 (for **1a**), CCDC-950235 (for **1b**), and CCDC-950236 (for **2a**) contain the supplementary crystallographic data (excluding structure factors) for this Article. These data can be obtained free of charge from The Cambridge Crystallographic Data Centre via www.ccdc.cam.ac.uk/data_request/cif.

■ ASSOCIATED CONTENT

Ⓢ Supporting Information

X-ray crystallographic data for complexes **I**, **1a**, **1b**, and **2a** in CIF format. Electronic absorption spectra of complexes **2b**−**5b** in different solvents, **2d** in CH_2Cl_2; emission spectra of complexes **1a**−**c**, **2a**, **2c**, and **3a**−**3c** at r.t. in solution; emission spectra of complexes **1a**−**1c**, **2a**−**2c**, **3a**−**3c**, **4a**, **4b**, **4e**, **5a**, **5b**, and **5e** at 77 K; crystal data and refinement details of complexes **I**, **1a**, **1b**, and **2b**; Cartesian coordinates and energies for all optimized molecules and spatial plots of selected frontier orbitals of the optimized ground state of **1b**−**5b**. This material is available free of charge via the Internet at http://pubs.acs.org.

■ AUTHOR INFORMATION

Corresponding Author

*E-mail: venkatesan.koushik@aci.uzh.ch.

Author Contributions

The manuscript was written through contributions of all authors. All authors have given approval to the final version of the manuscript.

Notes

The authors declare no competing financial interest.

■ ACKNOWLEDGMENTS

K.V. is grateful to Prof. H. Berke and Prof. R. Alberto for their generous support. This work was supported by the Swiss National Science Foundation (Grant 200021_135488) and University of Zürich.

■ REFERENCES

(1) (a) Baldo, M. A.; O'Brien, D. F.; You, Y.; Shoustikov, A.; Sibley, S.; Thompson, M. E.; Forrest, S. R. *Nature* **1998**, *395*, 151. (b) Thompson, M. *MRS Bull.* **2007**, *32*, 694. (c) Xiang, H.-F.; Lai, S.-W.; Lai, P. T.; Che, C.-M. In *Highly Efficient OLEDs with Phosphorescent Materials*; Wiley-VCH Verlag GmbH & Co. KGaA: New York, 2008; p 259. (d) Yersin, H.; Finkenzeller, W. J. In *Highly Efficient OLEDs with Phosphorescent Materials*; Wiley-VCH Verlag GmbH & Co. KGaA: New York, 2008; p 1. (e) Yersin, H.; Rausch, A. F.; Czerwieniec, R.; Hofbeck, T.; Fischer, T. *Coord. Chem. Rev.* **2011**, *255*, 2622. (f) Balzani, V.; Campagna, S.; Williams, J. A. G. In *Photochemistry and Photophysics of Coordination Compounds II*; Springer: Berlin, 2007; Vol. *281*, p 205. (g) Chi, Y.; Chou, P.-T. *Chem. Soc. Rev.* **2010**, *39*, 638. (h) Wong, W.-Y.; Ho, C.-L. *Acc. Chem. Res.* **2010**, *43*, 1246. (i) Currie, M. J.; Mapel, J. K.; Heidel, T. D.; Goffri, S.; Baldo, M. A. *Science* **2008**, *321*, 226. (j) Wong, W.-Y.; Harvey, P. D. *Macromol. Rapid Commun.* **2010**, *31*, 671. (k) Chan, C.-W.; Cheng, L.-K.; Che, C.-M. *Coord. Chem. Rev.* **1994**, *132*, 87. (l) Lu, W.; Mi, B.-X.; Chan, M. C. W.; Hui, Z.; Che, C.-M.; Zhu, N.; Lee, S.-T. *J. Am. Chem. Soc.* **2004**, *126*, 4958.

(2) (a) Li, K.; Guan, X.; Ma, C.-W.; Lu, W.; Chen, Y.; Che, C.-M. *Chem. Commun.* **2011**, *47*, 9075. (b) Wang, Z.; Turner, E.; Mahoney, V.; Madakuni, S.; Groy, T.; Li, J. *Inorg. Chem.* **2010**, *49*, 11276. (c) Hang, X.-C.; Fleetham, T.; Turner, E.; Brooks, J.; Li, J. *Angew. Chem., Int. Ed.* **2013**, *52*, 6753. (d) Han, J.; Chen, X.; Shen, L.; Chen, Y.; Fang, W.; Wang, H. *Chem.—Eur. J.* **2011**, *17*, 13971. (e) Rochester, D. L.; Develay, S.; Zalis, S.; Williams, J. A. G. *Dalton Trans.* **2009**, 1728. (f) Hanson, K.; Roskop, L.; Djurovich, P. I.; Zahariev, F.; Gordon, M. S.; Thompson, M. E. *J. Am. Chem. Soc.* **2010**, *132*, 16247.

(3) (a) Tsuboyama, A.; Iwawaki, H.; Furugori, M.; Mukaide, T.; Kamatani, J.; Igawa, S.; Moriyama, T.; Miura, S.; Takiguchi, T.; Okada, S.; Hoshino, M.; Ueno, K. *J. Am. Chem. Soc.* **2003**, *125*, 12971. (b) Yang, C.-H.; Tai, C.-C.; Sun, I. W. *J. Mater. Chem.* **2004**, *14*, 947. (c) Tamayo, A. B.; Alleyne, B. D.; Djurovich, P. I.; Lamansky, S.; Tsyba, I.; Ho, N. N.; Bau, R.; Thompson, M. E. *J. Am. Chem. Soc.*

2003, *125*, 7377. (d) Tsuzuki, T.; Shirasawa, N.; Suzuki, T.; Tokito, S. *Adv. Mater.* **2003**, *15*, 1455.
(4) (a) Unger, Y.; Zeller, A.; Ahrens, S.; Strassner, T. *Chem. Commun.* **2008**, 3263. (b) Unger, Y.; Meyer, D.; Molt, O.; Schildknecht, C.; Münster, I.; Wagenblast, G.; Strassner, T. *Angew. Chem., Int. Ed.* **2010**, *49*, 10214. (c) Unger, Y.; Meyer, D.; Strassner, T. *Dalton Trans.* **2010**, *39*, 4295. (d) Tronnier, A.; Strassner, T. *Dalton Trans.* **2013**, *42*, 9847.
(5) (a) Yang, X.; Wang, Z.; Madakuni, S.; Li, J.; Jabbour, G. E. *Adv. Mater.* **2008**, *20*, 2405. (b) Fleetham, T.; Wang, Z.; Li, J. *Org. Electron.* **2012**, *13*, 1430.
(6) Hudson, Z. M.; Sun, C.; Helander, M. G.; Chang, Y.-L.; Lu, Z.-H.; Wang, S. *J. Am. Chem. Soc.* **2012**, *134*, 13930.
(7) (a) Sajoto, T.; Djurovich, P. I.; Tamayo, A.; Yousufuddin, M.; Bau, R.; Thompson, M. E.; Holmes, R. J.; Forrest, S. R. *Inorg. Chem.* **2005**, *44*, 7992. (b) Yam, V. W.-W. *Acc. Chem. Res.* **2002**, *35*, 555. (c) Baggaley, E.; Weinstein, J. A.; Williams, J. A. G. *Coord. Chem. Rev.* **2012**, *256*, 1762. (d) Kalionowski, J.; Fattori, V.; Cocchi, M.; Williams, J. A. G. *Coord. Chem. Rev.* **2011**, *255*, 2401.
(8) Zhang, Y.; Garg, J. A.; Michelin, C.; Fox, T.; Blacque, O.; Venkatesan, K. *Inorg. Chem.* **2011**, *50*, 1220.
(9) (a) Unger, Y.; Zeller, A.; Taige, M. A.; Strassner, T. *Dalton Trans.* **2009**, 4786. (b) Muehlhofer, M.; Strassner, T.; Herdtweck, E.; Herrmann, W. A. *J. Organomet. Chem.* **2002**, *660*, 121.
(10) (a) Jahnke, M. C.; Pape, T.; Hahn, F. E. *Z. Naturforsch., B: Chem. Sci.* **2010**, 341. (b) Tanase, A. D.; Herdtweck, E.; Herrmann, W. A.; Kuehn, F. E. *Heterocycles* **2007**, *73*, 651.
(11) Gusev, D. G. *Organometallics* **2009**, *28*, 6458.
(12) (a) Vanhelmont, F. W. M.; Johnson, R. C.; Hupp, J. T. *Inorg. Chem.* **2000**, *39*, 1814. (b) Hissler, M.; Connick, W. B.; Geiger, D. K.; McGarrah, J. E.; Lipa, D.; Lachicotte, R. J.; Eisenberg, R. *Inorg. Chem.* **2000**, *39*, 447. (c) Wadas, T. J.; Chakraborty, S.; Lachicotte, R. J.; Wang, Q.-M.; Eisenberg, R. *Inorg. Chem.* **2005**, *44*, 2628. (d) Hua, F.; Kinayyigit, S.; Cable, J. R.; Castellano, F. N. *Inorg. Chem.* **2006**, *45*, 4304. (e) McGarrah, J. E.; Hupp, J. T.; Smirnov, S. N. *J. Phys. Chem. A* **2009**, *113*, 6430.
(13) (a) Farley, S. J.; Rochester, D. L.; Thompson, A. L.; Howard, J. A. K.; Williams, J. A. G. *Inorg. Chem.* **2005**, *44*, 9690. (b) Lai, S.-W.; Chan, M. C.-W.; Cheung, T.-C.; Peng, S.-M.; Che, C.-M. *Inorg. Chem.* **1999**, *38*, 4046. (c) Connick, W. B.; Geiger, D.; Eisenberg, R. *Inorg. Chem.* **1999**, *38*, 3264.
(14) (a) Yang, Q.-Z.; Wu, L.-Z.; Wu, Z.-X.; Zhang, L.-P.; Tung, C.-H. *Inorg. Chem.* **2002**, *41*, 5653. (b) Wen, H.-M.; Wu, Y.-H.; Fan, Y.; Zhang, L.-Y.; Chen, C.-N.; Chen, Z.-N. *Inorg. Chem.* **2010**, *49*, 2210.
(15) (a) Chan, C. K. M.; Tao, C.-H.; Tam, H.-L.; Zhu, N.; Yam, V. W.-W.; Cheah, K.-W. *Inorg. Chem.* **2009**, *48*, 2855. (b) Tao, C.-H.; Zhu, N.; Yam, V. W.-W. *Chem.—Eur. J.* **2005**, *11*, 1647.
(16) Frisch, M. J.; Trucks, G. W.; Schlegel, H. B.; Scuseria, G. E.; Robb, M. A.; Cheeseman, J. R.; Montgomery, J. A.; Vreven, T.; Kudin, K. N.; Burant, J. C.; Millam, J. M.; Iyengar, S. S.; Tomasi, J.; Barone, V.; Mennucci, B.; Cossi, M.; Scalmani, G.; Rega, N.; Petersson, G. A.; Nakatsuji, H.; Hada, M.; Ehara, M.; Toyota, K.; Fukuda, R.; Hasegawa, J.; Ishida, M.; Nakajima, T.; Honda, Y.; Kitao, O.; Nakai, H.; Klene, M.; Li, X.; Knox, J. E.; Hratchian, H. P.; Cross, J. B.; Bakken, V.; Adamo, C.; Jaramillo, J.; Gomperts, R.; Stratmann, R. E.; Yazyev, O.; Austin, A. J.; Cammi, R.; Pomelli, C.; Ochterski, J. W.; Ayala, P. Y.; Morokuma, K.; Voth, G. A.; Salvador, P.; Dannenberg, J. J.; Zakrzewski, V. G.; Dapprich, S.; Daniels, A. D.; Strain, M. C.; Farkas, O.; Malick, D. K.; Rabuck, A. D.; Raghavachari, K.; Foresman, J. B.; Ortiz, J. V.; Cui, Q.; Baboul, A. G.; Clifford, S.; Cioslowski, J.; Stefanov, B. B.; Liu, G.; Liashenko, A.; Piskorz, P.; Komaromi, I.; Martin, R. L.; Fox, D. J.; Keith, T.; Laham, A.; Peng, C. Y.; Nanayakkara, A.; Challacombe, M.; Gill, P. M. W.; Johnson, B.; Chen, W.; Wong, M. W.; Gonzalez, C.; Pople, J. A. *Gaussian 03*; Gaussian, Inc.: Wallingford, CT, 2003.
(17) Adamo, C.; Barone, V. J. *Chem. Phys.* **1999**, *110*, 6158.
(18) Dunning, T. H., Jr.; Hay, P. J. *Modern Theoretical Chemistry*; Schaefer, H. F., III, Ed.; Plenum: New York, 1976; Vol. 3, p 1.
(19) Ditchfield, R.; Hehre, W. J.; Pople, J. A. *J. Chem. Phys.* **1971**, *54*, 724.
(20) (a) Stratmann, R. E.; Scuseria, G. E.; Frisch, M. J. *J. Chem. Phys.* **1998**, *109*, 8218. (b) Bauernschmitt, R.; Ahlrichs, R. *Chem. Phys. Lett.* **1996**, *256*, 454. (c) Casida, M. E.; Jamorski, C.; Casida, K. C.; Salahub, D. R. *J. Chem. Phys.* **1998**, *108*, 4439.
(21) (a) Barone, V.; Cossi, M. *J. Phys. Chem. A* **1998**, *102*, 1995. (b) Cossi, M.; Rega, N.; Scalmani, G.; Barone, V. *J. Comput. Chem.* **2003**, *24*, 669.
(22) Diez-Barra, E.; de la Hoz, A.; Rodriguez-Curiel, R.; Tejeda, J. *Tetrahedron* **1997**, *53*, 2253.
(23) Agilent Technologies (formerly Oxford Diffraction), Yarnton, Oxfordshire, England, 2012.
(24) Clark, R. C.; Reid, J. S. *Acta Crystallogr., Sect. A.* **1995**, *51*, 887.
(25) *CrysAlisPro Version 1.171.36.20*; Agilent Technologies: Yarnton, Oxfordshire, England, 2012.
(26) Dolomanov, O. V.; Bourhis, L. J.; Gildea, R. J.; Howard, J. A. K.; Puschmann, H. *J. Appl. Crystallogr.* **2009**, *42*, 339.
(27) Sheldrick, G. M. *Acta Crystallogr., Sect. A.* **2008**, *64*, 112.
(28) Spek, A. L. *J. Appl. Crystallogr.* **2003**, *36*, 7.